

# Joint Antenna Position and Beamforming Optimization for Movable Antenna Enabled Secure IRS-ISAC Network

Xiaowen Cao, *Member, IEEE*, Peng Jiang, Guangxu Zhu, *Member, IEEE*,  
Yejun He, *Senior Member, IEEE*, and Moshen Guizani, *Fellow, IEEE*

**Abstract**—Integrated sensing and communication (ISAC) can effectively improve the spectrum utilization rate and enhance the system performance. This paper focuses on the secure communication problem in an ISAC system, which consists of a base station (BS), a legitimate user, an eavesdropping target, and an intelligent reflecting surfaces (IRS). To further investigate the impact of channel reconfigurability on the security performance of the ISAC system, movable antennas (MA) are employed at the BS instead of traditional fixed antennas. We aim to jointly design the communication transmit beamforming at the BS, the sensing covariance matrix, the phase shifts of the IRS, and the positions of the MAs to ensure secure communication for the user equipment (UE), subject to constraints including the maximum transmit power at the BS, the constant-modulus constraint of the IRS, the minimum spacing requirement between MAs, and the sensing beam gain constraint. To address the non-convex optimization problem, we adopt an alternating optimization algorithm. Specifically, by combining successive convex approximation (SCA) and semidefinite relaxation (SDR) techniques, the problems of designing the transmit beamforming matrix at the BS and the phase shifts of the IRS are transformed into convex optimization problems. Subsequently, a particle swarm optimization (PSO) algorithm is used to optimize the positions of the MA. Simulation results demonstrate the effectiveness of the IRS in improving the system performance and highlight the superiority of the MA in improving security compared to traditional ISAC systems.

**Index Terms**—Integrated sensing and communication, movable antenna, intelligent reflecting surface, physical layer security, particle swarm optimization.

The work was supported in part by National Key Research and Development Program of China under Grant No. 2023YFE0107900, National Natural Science Foundation of China under Grants Nos. 62501407, 62371313, and 62071306, Shenzhen Science and Technology Program under Grant No. RCBS20231211090520032, Guangdong Young Talent Research Project under Grant No. 2023TQ07A708, Guangdong Provincial Key Laboratory of Future Networks of Intelligence under Grant No. 2022B1212010001, Shenzhen Key Program of Natural Science Foundation under Grant No. JCYJ20241202124219023, and in part by the Guangdong Provincial Key Laboratory of Future Networks of Intelligence, The Chinese University of Hong Kong, Shenzhen, under Grant No. 2022B1212010001. (Corresponding author: Yejun He.)

Xiaowen Cao, Peng Jiang, and Yejun He are with the State Key Laboratory of Radio Frequency Heterogeneous Integration, Sino-British Antennas and Propagation Joint Laboratory of MOST, Guangdong Engineering Research Center of Base Station Antennas and Propagation, Shenzhen Key Laboratory of Antennas and Propagation, College of Electronics and Information Engineering, Shenzhen University, Shenzhen 518060, China (e-mail: caoxwen@szu.edu.cn; 1044609737@qq.com; heyejun@126.com);

Xiaowen Cao is also with the Guangdong Provincial Key Laboratory of Future Networks of Intelligence, The Chinese University of Hong Kong, Shenzhen 518172, China.

Guangxu Zhu is with Shenzhen Research Institute of Big Data, Shenzhen 518172, China (email: gxzhu@sribd.cn).

Moshen Guizani is with the Mohamed Bin Zayed University of Artificial Intelligence (MBZUAI), UAE (email: mguizani@ieee.org).

## I. INTRODUCTION

NEXT-generation wireless networks demand substantially enhanced sensing and communication capabilities to support a plethora of emerging applications [1]. To enhance the high-precision sensing prowess within wireless systems, integrated sensing and communication (ISAC), widely acknowledged as one of the pivotal enabling technologies for sixth-generation (6G) wireless networks, has attracted remarkable attention and spurred extensive research endeavors [2]–[4]. A promising emerging research direction in ISAC is edge perception [5], which refers to the integration of ISAC with edge learning [6], [7]. This fusion brings AI-driven sensing and decision-making closer to end devices, laying the foundation for advanced applications such as smart manufacturing, autonomous vehicles, and intelligent transportation systems. Related work [8]–[10] focused on edge computing scenarios and the field of integration of communication and intelligence, committed to improving the efficiency and stability of systems. However, to implement ISAC in practice, it still faces some challenges. First, the physical-layer trade-offs between communication and sensing (such as detection and communication [11] or estimation and communication [12]) are hard to be characterized within a uniform framework, due to the different resource allocation requirements like in spatial degrees of freedom. Then, ISAC systems may inherit vulnerabilities from conventional wireless networks, leading to a degradation on sensing accuracy or misleading perception-driven applications.

In particular, physical layer security (PLS) has gained attraction as a promising approach to safeguard transmissions by leveraging the randomness and spatial diversity inherent in wireless channels [13], [14]. Existing techniques, such as artificial noise injection [15], channel-based secret key generation [16], and cooperative jamming [17] have been widely adopted to enhance security in wireless networks. Meanwhile, secure beamforming [18] also plays a central role by precisely shaping the transmission pattern to enhance the desired signal quality, thus ensuring confidentiality of the physical layer. However, traditional secure beamforming designs mainly rely on fixed antennas (FPA). In this case, the positions of the antennas at transmitter/receiver cannot be changed [19]. This brings about a distinct drawback, that is, when the direction of the eavesdropper is close to the azimuth angle at which the legitimate user receives the signal, the channel correlation between the user channel and the eavesdropping channel

will increase significantly [20], making it difficult for the beamforming technology to distinguish between legitimate and illegal users. Therefore, a novel antenna technology movable antenna (MA) has been proposed in some research. Specifically, MA connected to the radio frequency link through a flexible cable and enabled to move via a mechanical device [21], simultaneously provides additional degrees of freedom.

In the security design of ISAC systems, intelligent reflecting surfaces (IRS) are often considered as emerging technologies [22]. Through the independent tuning of passive reflecting elements, IRS adjusts incident electromagnetic waves to adapt to the variations in the wireless environment, thereby achieving expanded coverage [23], improved channel quality [24], and interference mitigation [25]. In situations where the direct line-of-sight (LoS) path between the base station, the user, and the target is obstructed, establishing a virtual LoS link via the IRS can enhance the stability and reliability of a signal transmission. Additionally, through the passive beamforming design of IRS elements, it will further boost the gain for legitimate communication users while decreasing the gain for illegal targets.

IRS-assisted ISAC systems have become a research hotspot in both academia and industry. Leveraging the tunable characteristics of IRS on wireless channels, this technology can effectively enhance the joint communication and sensing performance of ISAC systems: on the one hand, it can expand the applicable scenarios of the system by utilizing the property of diffracting obstacles; on the other hand, it can optimize the system efficiency through dynamic resource scheduling and expand the signal coverage area. However, IRS-assisted ISAC systems still face many challenges, such as high complexity of the channel estimation, great difficulty in engineering implementation of hardware deployment, and complexity of the system-level interference management. It is worth noting that the dynamic regulation capability of IRS on channel characteristics also provides a new technical path for improving the security performance of ISAC systems.

#### A. Related Work

1) *PLS*: In research related to PLS, some research attempts are committed to ensuring the security performance of the system by maximizing the secrecy energy efficiency [26], [27]. Specifically, in [26], the secrecy energy efficiency of primary users was guaranteed by jointly designing the artificial noise vector and discrete phase shift of the IRS. Furthermore, the work in [27] considered a visible light communication network and focused on exploring the approach to optimize the performance of secrecy energy efficiency. The authors in [28] discussed ensuring the security of unmanned aerial vehicle (UAV) communication through cooperative jamming and trajectory control, while they further considered a power adaptation scheme in the 3D state and introduced multi-point cooperation [29]. Furthermore, the work [30] investigated the security transmission problem in UAV-assisted mobile edge computing based on reinforcement learning. Assisted by IRS technology, the work [32] optimized the security performance in a healthcare network with the assistance of

the IRS, while authors in [31] used a hybrid deep reinforcement learning method to address the security issues in air-ground communication, improving the communication security performance through multi-UAV cooperation. From the perspective of jamming and beamforming in communication security, robust security of UAV communication is achieved through the design of jamming beamforming in [33], and [34] combined the IRS with non-orthogonal multiple access (NOMA) to achieve secure transmission through adaptive jamming beamforming. The advantages of IRS-UAV for ISAC and related typical technologies are introduced, and different optimization schemes are proposed to address jamming and eavesdropping attacks [36]. Taking into account the imperfect sensing estimation, from the new perspective of combining ISAC and IRS technologies, it could provide a more in-depth research direction for communication security [35].

In some relevant studies on the security performance of ISAC systems, authors of [37] and [38] considered the scenario where the targets are eavesdroppers and assumed that the non-ideal channel state information can be obtained. They respectively proposed a robust scheme for ISAC systems to improve secure communication and sensing services. The systems studied are mainly in the state where communication and radar work independently rather than cooperatively. In the cooperative state, [39] realized a secure transmission of ISAC systems by optimizing resource allocation design.

2) *IRS-aided ISAC Secure Transmission*: Currently, there have been many studies utilizing the IRS to assist in enhancing the security performance of the ISAC system [40]–[50]. In terms of the related scheme design, the study [40] proposed a semi-passive IRS-aided ISAC scheme. For the two scenarios of point targets and extended targets, it aims to maximize the secrecy rate while minimizing the Cramér-Rao (CRB) bound. In the research on the combination of unmanned aerial vehicles (UAVs) and the ISAC network, the work [41] deployed the IRS on UAVs. By leveraging the high-altitude characteristics of UAVs, LoS links were established, thus expanding the coverage area. Moreover, another investigation [42] combined the ISAC base station (BS) with UAVs, enhanced the signal strength through the IRS, and jointly optimized phase shifts of the IRS and the trajectories of the UAVs. In scenarios where the LoS links are obstructed, the authors in [43] utilized the links established by the IRS to realize the virtual LoS link survey of illegal targets that are difficult for the BS to detect. Additionally, the research in the non-orthogonal multiple access system [44], through jointly designing the phase shifts of the IRS and artificial jamming, can achieve target detection while ensuring the secure communication of users. In the work [45], the authors studied the IRS-aided ISAC system, taking into account multistatic cooperative sensing. By utilizing the shared azimuth angles, they achieved the localization of the eavesdropping target. Based on the positioning information obtained from the sensing, they optimized the communication transmission beamforming to realize secure communication. In the research on some new types of IRS-aided ISAC systems, authors of [46] and [47] utilized the simultaneously transmitting and reflecting reconfigurable intelligent surface (STAR) to assist in the research on the

TABLE I: Comparison of related works with our work

Reference	IRS	MA	ISAC	Security	Objective Function	Sensing Metric	Communication Metric	Optimization Method
[26]	✓	×	×	✓	Communication metric	–	Secrecy energy efficiency	DRL
[27]	×	×	×	✓	Communication metric	–	Secrecy rate	SCA
[31]	✓	×	×	✓	Communication metric	–	Secrecy rate	DRL
[33]	×	×	×	✓	Communication metric	–	Sum secrecy rate	SCA/SDR
[40]	✓	×	✓	✓	Communication metric	CRB	Secrecy rate	SCA/SDR
[42]	✓	×	✓	✓	Communication metric	Echo SNR	Sum secrecy rate	SCA
[43]	✓	×	✓	✓	Communication metric	Echo SNR	Sum secrecy rate	SCA
[44]	✓	×	✓	✓	Sensing metric	Beam pattern gain	SINR	Penalty-based
[45]	✓	×	✓	✓	Communication metric	Estimated localization	Sum secrecy rate	SCA
[50]	✓	×	✓	✓	Communication metric	Echo SINR	Secrecy rate	DRL
[51]	×	✓	×	✓	Communication metric	–	Beam gain	Closed form
[52]	×	✓	×	✓	Communication metric	–	Secrecy rate	Gradient descent
[53]	×	✓	×	×	Communication metric	–	Sum data rate	SCA
[54]	×	✓	×	×	Communication metric	–	Transmit power	Generalized Benders
[57]	✓	✓	✓	×	Both metrics	–	Sum communication rate	KKT/DCA
[58]	×	✓	✓	×	Sensing metric	CRB	SINR	SCA
[59]	✓	✓	✓	×	Sensing metric	–	SINR	SCA
Proposed	✓	✓	✓	✓	Communication metric	Beam pattern gain	Secrecy rate	SCA/PPO

Note: DGA: Direct gradient descent; KKT: Karush-Kuhn-Tucker.

security performance of the IRS-ISAC system. The authors in [48] [49] replace the passive IRS with the active IRS, achieving the phase modulation of the incident signal and simultaneously amplifying the signal. Furthermore, the soft-actor critical algorithm in reinforcement learning was applied to enhance the security of IRS-supported ISAC systems as described in [50].

3) *Beamforming and Position Optimization for MA*: Current research on MA in MA-assisted communication systems mainly centers on two crucial aspects: Beamforming design [51], [52] and MA position optimization [53], [54]. The seminal work [19] devised a channel estimation framework for MA systems based on field responses. It also developed a computational method to analyze channel responses under different MA setups within factory environments.

Recent studies have combined MA with IRS to leverage channel reconfigurability. The work [55] presented a coordinated MA-IRS system that reduces the user-side signal-to-interference-plus-noise ratio (SINR) by dynamically positioning antennas on IRS surfaces. Authors in [56] explored enhancements for internet of things networks through joint MA-IRS reconfiguration strategies, which dynamically reshape propagation environments to enhance channel conditions.

Existing studies have systematically explored the spatial advantages of MA over FPA in ISAC systems. These investigations demonstrate significant benefits, including enhanced sensing beam gain [57]–[60] and optimized communication performance under sensing constraints [61]–[63]. Specifically, work [58] implements MA configurations at both BS and user terminals, deriving CRB position relationships and formulating a constrained CRB minimization framework. Under the constraint of communication SINR, authors in [59] and [60] respectively achieved the maximization of the radar SINR and the maximization of the minimum radar beam gain through the joint optimization of transmit beamforming and antenna positions. The author in [61] proposed an effective framework

to enhance the communication SINR and the beam pattern gain. The work in [62] achieved a significant improvement in the communication rate and sensing mutual information of ISAC compared to fixed uniform arrays. The bistatic ISAC analysis in [63] decomposes a joint optimization into four coupled subproblems using MA arrays and dual performance metrics. However, in the studies mentioned above, the impact of the channel reconfigurability introduced by MA and IRS on the security performance of ISAC systems has not been thoroughly investigated. The comparison between related work and our work is shown in Table I.

## B. Motivation and Contribution

To comprehensively harness the synergistic channel reconfigurability offered by IRS and MA, this paper delves into the realm of secure communication within IRS-enabled ISAC systems with MA assistance. In these systems, the ISAC BS, outfitted with MA, is tasked with the dual challenge of detecting potential targets that may concurrently function as eavesdroppers and ensuring the uninterrupted communication with legitimate users. Additionally, given that the LoS paths between the BS, the user, and the target are obstructed by physical blockers, the reconstruction of the communication link through the IRS becomes imperative. The principal contributions of this paper are summarized as follows

- We aim to jointly optimize the transmit beamforming vector, IRS phase shift configuration, and BS-mounted MA positions, while satisfying the maximum transmit power constraints, IRS unit-modulus phase shift constraints, antenna displacement spatial constraints, and minimum beam pattern gain constraints. The inherent strong coupling among optimization variables induces non-convex inter-dependencies in the objective function, rendering the joint optimization problem mathematically intractable.

- To tackle the above challenge, we propose an alternating optimization algorithm. The original problem is decoupled into two subproblems, which respectively target the joint transmit beamforming, IRS phase shift design, and antenna position optimization. Specifically, when the positions of MAs are fixed, the first subproblem is further decomposed into two mutually coupled modules. In the first sub-module, the successive convex approximation (SCA) and semidefinite relaxation (SDR) techniques are utilized to transform the relevant problems into tractable convex problems. Subsequently, based on the obtained transmit beamforming matrix, SCA and sparse reconstruction conjugate rank (SRCR) techniques are combined to transform the IRS phase shift design problem into a convex problem. Finally, the PSO algorithm is used to perform a metaheuristic-driven stochastic search, iteratively optimizing the positions of MAs based on the given beamforming vectors and IRS phase shifts.
- The simulation results demonstrate the effectiveness of the MAs-assisted IRS-ISAC system in enhancing security. Meanwhile, compared with the traditional FPA, it can achieve higher security performance.

### C. Organization

The remainder of this paper is structured as follows. Section II details the system model and formulates the associated problems. Subsequently, in Section III, we put forward the PSO-AO solution. Moving on to Section VI, a series of simulations are carried out to showcase the performance of the proposed solution. Finally, the conclusion is presented in Section VII.

**Notation:** The bold-face lower-case and upper-case letters denote the vectors and matrices, respectively.  $|a|$  represents the absolute value of  $a$ .  $\text{diag}\{\mathbf{a}\}$  represents a diagonal matrix where the elements of vector  $\mathbf{a}$  are placed on the main diagonal.  $(\cdot)^T$  and  $(\cdot)^H$  represent the transpose and hermitian transpose, respectively.  $\lfloor \cdot \rfloor$  denotes the floor function.  $\mathbb{E}(\cdot)$  denotes the statistical expectation.  $\mathcal{CN}(0, \sigma^2)$  represents a complex circularly symmetric Gaussian distribution with a mean of zero and a variance of  $\sigma^2$ .  $\text{Tr}(\mathbf{A})$  represents the trace operation of matrix  $\mathbf{A}$ .  $[\cdot]^+ = \max\{\cdot, 0\}$ .  $\nabla_{\mathbf{W}}^H f(\mathbf{W}, \mathbf{R}_r)$  represents the conjugate transpose of the gradient of the function  $f(\cdot)$  with respect to the matrix  $\mathbf{W}$ .

## II. SYSTEM MODEL

As shown in Fig. 1, we consider a secure IRS-ISAC scenario, where ISAC needs to communicate with a user under the assistance of IRS and sense an environmental target. A BS equipped with a linear MA transmit array of length  $J$ , along which the positions of the  $M$  antennas can be adjusted flexibly. While the BS is communicates with the legitimate user (Bob) equipped with a single antenna, the BS needs to sense the target located at the non-line-of-sight (NLoS) link. Assume that this target (Eve) also has a single antenna and attempts to intercept Bob's data. Direct links between the BS and user/target are assumed to be unfavorable due to blockages. As a result, the IRS is responsible for generating strong virtual

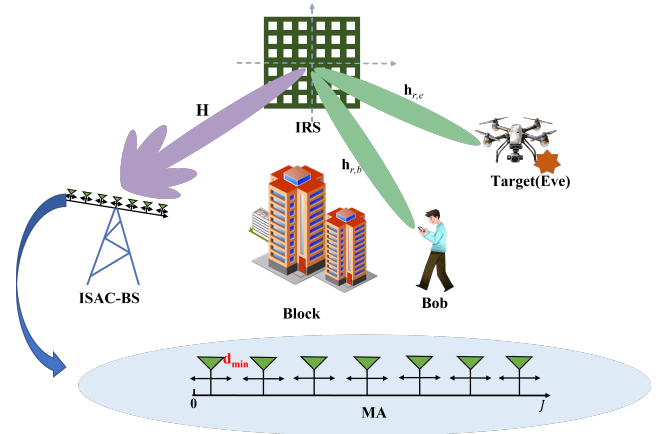


Fig. 1: Illustration of the IRS-ISAC system, where the BS is equipped with MAs.

LoS links to support communication and sensing performance. The IRS is a uniform planar array with  $N$  reflecting elements. The antenna position vector of the linear MA array in the BS can be represented as  $\mathbf{t} = [t_1, t_2, \dots, t_M]^T \in \mathbb{R}^M$ , where  $t_m$  denotes the coordinates of the  $m$ -th antenna. The sets of MA of BS and IRS as  $\mathcal{M} = \{1, \dots, M\}$  and  $\mathcal{N} = \{1, \dots, N\}$ . To mitigate the mutual coupling between antennas of finite size, a minimum distance  $d_{\min}$  is imposed between any two antennas. Thus, the condition must be satisfied

$$|t_i - t_j| \geq d_{\min}, \forall i, j \in \mathcal{M}, i \neq j. \quad (1)$$

### A. Channel Model

Considering the planar far-field channel model, each transmit/receive path within the same channel shares a common angle of departure, angle of arrival, and path response coefficient, but with distinct signal phases. For simplicity, it is assumed that all channels are with undergo quasi-static flat-fading and the CSI of all channels involved is perfectly known at both the BS and the IRS. Thus, the channel between the IRS and the BS can be expressed as  $\mathbf{H}(\mathbf{t}) = \mathbf{G}(\mathbf{t})^H \mathbf{\Lambda}^H \mathbf{F} \in \mathbb{C}^{M \times N}$ . The notations mentioned are defined as

- $\mathbf{G}(\mathbf{t}) = [\mathbf{G}_1(t_1), \dots, \mathbf{G}_m(t_m), \dots, \mathbf{G}_M(t_M)] \in \mathbb{C}^{L \times M}$  is the transmit field response vector (FRV) in the BS, where  $L$  denotes the number of channel paths between the BS and the IRS. Each  $\mathbf{G}_m \in \mathbb{C}^{L \times 1}$  corresponds to the transmit FRV from the  $m$ -th MA and the IRS for  $m \in \mathcal{M}$ .
- $\mathbf{G}_m(t_m) = [e^{j \frac{2\pi}{\lambda} t_m \cos \theta_{m,1}}, \dots, e^{j \frac{2\pi}{\lambda} t_m \cos \theta_{m,L}}]^H$ , where  $\theta_{m,l} \in [0, 2\pi]$  is the elevation angles of the  $l$ -th path for the  $m$ -th antennas for  $l = 1, \dots, L$ , and  $\lambda$  is the wavelength.
- $\mathbf{\Lambda} = \text{diag}\{\nu_1, \dots, \nu_L\} \in \mathbb{C}^{L \times L}$ , where  $\nu_l$  is the complex response of the path  $l$ .
- $\mathbf{F} = [\mathbf{f}(\mathbf{r}_1), \dots, \mathbf{f}(\mathbf{r}_n), \dots, \mathbf{f}(\mathbf{r}_N)] \in \mathbb{C}^{L \times N}$  is the receive FRV of the IRS, and  $\mathbf{r}_n = (x_n, y_n)$  represents the  $n$ -th coordinates of the reflection element.  $\mathbf{f}(\mathbf{r}_n) = [e^{j \frac{2\pi}{\lambda} \rho_r^1(\mathbf{r}_n)}, e^{j \frac{2\pi}{\lambda} \rho_r^2(\mathbf{r}_n)}, \dots, e^{j \frac{2\pi}{\lambda} \rho_r^L(\mathbf{r}_n)}]^T \in \mathbb{C}^{L \times 1}$ , where  $\rho_r^i(\mathbf{r}_n) = x_n + \sin \theta_i^r \cos \psi_i^r + y_n \cos \theta_i^r$  is the difference in the propagation distance of the signal

for the  $i$ -th receiving path between the position of the element  $\mathbf{r}_n$  and the origin of the IRS. Here,  $\psi_i^r$  and  $\theta_i^r$  are the elevation and azimuth angles of the  $i$ -th receiving path at the IRS, respectively.

The channel between the IRS to Bob  $\mathbf{h}_{r,b} \in \mathbb{C}^{N \times 1}$  follows the Rician fading, which can be given by

$$\mathbf{h}_{r,b} = \sqrt{\iota d_{r,b}^{-2.2}} \left( \sqrt{\frac{\kappa}{\kappa+1}} \mathbf{h}_{r,b}^{\text{LoS}} + \sqrt{\frac{1}{\kappa+1}} \mathbf{h}_{r,b}^{\text{NLoS}} \right), \quad (2)$$

where  $\iota$  denotes the path loss factor at the reference distance  $\iota_0 = 1$  m,  $d_{r,b}$  represents the distance between the IRS and Bob, and  $\kappa$  stands for the Rician factor.  $\mathbf{h}_{r,b}^{\text{NLoS}} \sim \mathcal{CN}(0, \mathbf{I})$  denotes the NLoS component. Given the azimuth  $\theta_{r,b} \in (0, 2\pi]$  and the elevation angle  $\zeta_{r,b} \in (-\pi/2, \pi/2]$  from the IRS to the user, in accordance with [64], the LoS component is expressed as  $\mathbf{h}_{r,b}^{\text{LoS}}$ , and its  $n$ -th elements  $[\mathbf{h}_{r,b}^{\text{LoS}}]_n$ , is given by

$$[\mathbf{h}_{r,b}^{\text{LoS}}]_n = e^{j2\pi d_r (\lfloor \frac{n}{N_x} \rfloor \eta_{b,1} + (n - \lfloor \frac{n}{N_x} \rfloor N_x) \eta_{b,2}) / \lambda}, \forall n \in \mathcal{N}, \quad (3)$$

where  $\eta_{b,1} = \sin(\theta_{r,b}) \sin(\zeta_{r,b})$ ,  $\eta_{b,2} = \sin(\theta_{r,b}) \cos(\zeta_{r,b})$ ,  $N_x$  denotes the count of IRS elements in each row, and  $d_r$  is the space between adjacent reflecting elements.

Assume that the virtual LoS channel created by the IRS is stronger than the NLoS channel. Let  $\theta_{r,e}$  and  $\zeta_{r,e}$  represent the azimuth angle and departure angle of the target relative to the IRS, respectively. Similarity, the steering vector between the IRS and the target can be expressed as  $\mathbf{a} \in \mathbb{C}^{N \times 1}$ , and its  $n$ -th element steering vector  $[\mathbf{a}]_n$  is given by

$$[\mathbf{a}]_n = e^{j2\pi d_r (\lfloor \frac{n}{N_x} \rfloor \eta_{e,1} + (n - \lfloor \frac{n}{N_x} \rfloor N_x) \eta_{e,2}) / \lambda}, \forall n \in \mathcal{N}, \quad (4)$$

where  $\eta_{e,1} = \sin(\theta_{r,e}) \sin(\zeta_{r,e})$ ,  $\eta_{e,2} = \sin(\theta_{r,e}) \cos(\zeta_{r,e})$ . Thus, the channel between the IRS and Eve can be expressed as  $\mathbf{h}_{r,e} = \sqrt{\iota d_{r,e}^{-2.2}} \mathbf{a}(\theta_{r,e}, \zeta_{r,e}) \in \mathbb{C}^{N \times 1}$ , where  $d_{r,e}$  represents the distance between the IRS and Eve.

### B. Signal Model

Let  $s_c \sim \mathcal{CN}(0, 1)$  represent the communication signal transmitted to Bob,  $\mathbf{x}_r \in \mathbb{C}^{M \times 1}$  denote the sensing signal vector, which is generated independently of the communication signals. The covariance matrix of  $\mathbf{x}_r$  is

$$\mathbf{R}_r \triangleq \mathbb{E}(\mathbf{x}_r \mathbf{x}_r^H) \succeq 0. \quad (5)$$

The transmit signal of the ISAC BS is represented as

$$\mathbf{x} = \mathbf{w}_c s_c + \mathbf{x}_r, \quad (6)$$

where  $\mathbf{w}_c \in \mathbb{C}^{M \times 1}$  denote the beamforming matrices for the communication. The covariance matrix  $\mathbf{R}_x$  of the transmitted signal  $\mathbf{x}$  can be expressed as

$$\mathbf{R}_x = \mathbb{E}(\mathbf{x} \mathbf{x}^H) = \mathbf{w}_c \mathbf{w}_c^H + \mathbf{R}_r. \quad (7)$$

The beamforming gain  $\mathcal{P}(\mathbf{w}_c, \mathbf{R}_r, \Phi, \mathbf{t})$  in the sensing direction  $\theta_{r,e}$  as the radar performance metric and can be expressed as

$$\begin{aligned} \mathcal{P}(\mathbf{w}_c, \mathbf{R}_r, \Phi, \mathbf{t}) &= \mathbb{E} \left( |\mathbf{h}_{r,e}^H \Phi \mathbf{H}(\mathbf{t})^H \mathbf{x}|^2 \right) \\ &= \mathbf{h}_{r,e}^H \Phi \mathbf{H}(\mathbf{t})^H (\mathbf{w}_c \mathbf{w}_c^H + \mathbf{R}_r) \mathbf{H}(\mathbf{t}) \Phi^H \mathbf{h}_{r,e}, \end{aligned} \quad (8)$$

where  $\Phi = \text{diag}(\varphi_1, \dots, \varphi_n, \dots, \varphi_N)$  represents the phase shift matrix of the IRS with  $\varphi_n = \xi_n e^{j\vartheta_n}$ ,  $\xi_n \in [0, 1]$  represents the amplitude reflection coefficient, and  $\vartheta_n \in (0, 2\pi]$  denotes the phase shift of the  $n$ -th reflecting element. For simplicity, the amplitude effect of the IRS is ignored, i.e.,  $\xi_n = 1, \forall n \in \mathcal{N}$  [65].

The received signal at Bob and Eve can be obtained as

$$y_i = \mathbf{h}_i^H \Phi \mathbf{H}(\mathbf{t})^H \mathbf{x} + n_i, i \in \{b, e\}, \quad (9)$$

where  $n_b, n_e \sim \mathcal{CN}(0, \sigma^2)$  represents the received noise at Bob and Eve. Let  $\mathbf{h}_b(\Phi, \mathbf{t}) = \mathbf{H}(\mathbf{t}) \Phi^H \mathbf{h}_{r,b}$  and  $\mathbf{h}_e(\Phi, \mathbf{t}) = \mathbf{H}(\mathbf{t}) \Phi^H \mathbf{h}_{r,e}$  denote the equivalent channels from the BS to Bob and the BS to Eve, respectively. Then, the achievable data rate  $R_b(\mathbf{w}_c, \mathbf{R}_r, \Phi, \mathbf{t})$  for Bob can be expressed as

$$R_b(\mathbf{w}_c, \mathbf{R}_r, \Phi, \mathbf{t}) = \log_2 \left( 1 + \frac{|\mathbf{h}_b(\Phi, \mathbf{t})^H \mathbf{w}_c|^2}{\mathbf{h}_b(\Phi, \mathbf{t})^H \mathbf{R}_r \mathbf{h}_b(\Phi, \mathbf{t}) + \sigma^2} \right). \quad (10)$$

Similarly, the eavesdropping data rate  $R_e(\mathbf{w}_c, \mathbf{R}_r, \Phi, \mathbf{t})$  for Eve to intercept the information intended for Bob is given by

$$R_e(\mathbf{w}_c, \mathbf{R}_r, \Phi, \mathbf{t}) = \log_2 \left( 1 + \frac{|\mathbf{h}_e(\Phi, \mathbf{t})^H \mathbf{w}_c|^2}{\mathbf{h}_e(\Phi, \mathbf{t})^H \mathbf{R}_r \mathbf{h}_e(\Phi, \mathbf{t}) + \sigma^2} \right). \quad (11)$$

Thus, the system's secure rate  $R_{sec}(\mathbf{w}_c, \mathbf{R}_r, \Phi, \mathbf{t})$  is formulated as

$$R_{sec}(\mathbf{w}_c, \mathbf{R}_r, \Phi, \mathbf{t}) = [R_b(\mathbf{w}_c, \mathbf{R}_r, \Phi, \mathbf{t}) - R_e(\mathbf{w}_c, \mathbf{R}_r, \Phi, \mathbf{t})]^+ \quad (12)$$

### C. Problem Formulation

The objective in this work is to maximize the secure rate by jointly designing the transmit beamforming  $\mathbf{w}_c$ , the covariance matrix  $\mathbf{R}_r$ , the phase shift matrix  $\Phi$ , and the MA's position  $\mathbf{t}$ .

$$\begin{aligned} \text{(P1)} : \quad & \max_{\mathbf{w}_c, \mathbf{R}_r, \Phi, \mathbf{t}} R_{sec}(\mathbf{w}_c, \mathbf{R}_r, \Phi, \mathbf{t}) \\ \text{s.t.} \quad & \mathcal{P}(\mathbf{w}_c, \mathbf{R}_r, \Phi, \mathbf{t}) \geq \varepsilon, \quad (13a) \\ & \|\mathbf{w}_c\|^2 + \text{Tr}(\mathbf{R}_r) \leq P_{\max}, \quad (13b) \\ & \mathbf{R}_r \succeq 0, \quad (13c) \\ & \Phi = \text{diag}(e^{j\vartheta_1}, \dots, e^{j\vartheta_N}), \quad (13d) \\ & |t_i - t_j| \geq d_{\min}, \forall i, j \in \mathcal{M}, i \neq j, \quad (13e) \\ & t_m \in [0, J], \forall m \in \mathcal{M}. \quad (13f) \end{aligned}$$

The radar beamforming gain is specified in the constraint (13a), where  $\varepsilon$  represents the minimum required radar beamforming. Constraint (13b) denotes the transmission power budget at the BS, with  $P_{\max}$  representing the maximum transmission power. Additionally, constraint (13d) addresses the phase shift constraints of the IRS, while constraints (13e) and (13f) represent the MA position constraints. It is observed that problem (P1) is highly non-convex due to the non-convex objective functions and constraints among coupling variables.

### III. PROBLEM OPTIMIZATION

In this part, we divide the original problem into two subproblems. Under any given antenna position, we optimize  $\mathbf{w}_c, \mathbf{R}_r, \Phi$ , by leveraging the SDR and SCA techniques. Then, with the obtained  $\mathbf{w}_c, \mathbf{R}_r, \Phi$ , we use the PSO to optimize the antenna position.

### A. Performance Optimization under Given Antenna Position

Given the antenna positions, the primary problem is reduced to

$$\begin{aligned}
 \text{(P2)} : \quad & \max_{\mathbf{w}_c, \mathbf{R}_r, \Phi} R_{sec}(\mathbf{w}_c, \mathbf{R}_r, \Phi) \\
 \text{s.t.} \quad & \mathbf{h}_e^H (\mathbf{w}_c \mathbf{w}_c^H + \mathbf{R}_r) \mathbf{h}_e \geq \varepsilon, \quad (14a) \\
 & \|\mathbf{w}_c\|^2 + \text{Tr}(\mathbf{R}_r) \leq P_{\max}, \quad (14b) \\
 & \mathbf{R}_r \succeq \mathbf{0}, \quad (14c) \\
 & \Phi = \text{diag}(e^{j\vartheta_1}, \dots, e^{j\vartheta_N}). \quad (14d)
 \end{aligned}$$

This problem is still non-convex. Similarly, we decompose this problem into two sub-problems, namely the joint optimization problem of the communication beamforming and the sensing covariance matrix, and the IRS phase-shift design problem. For the first sub-problem, we adopt a hybrid approach combining SCA and SDR. Specifically, we first apply SDR to relax the rank-one constraint, transforming the non-convex problem into a tractable problem. The SDR algorithm relaxes non-convex quadratic optimization problems by replacing the rank-one constraint with positive semidefinite constraints, yielding both a lower bound on the optimal value and approximate solutions via techniques like Gaussian randomization. Subsequently, we use a rank-one reconstruction method to enforce the rank constraint approximately, ensuring the solution quality. For the second sub-problem, we employ a similar SCA-SDR framework. However, due to the limitations of the traditional Gaussian randomization in recovering rank-one solutions, we leverage the Successive Rank-Constrained Relaxation (SRCR) algorithm. The SRCR iteratively refines solutions while respecting the rank constraint, outperforming standard randomization methods in certain scenarios.

1) *Optimization of Beamforming Vector and Radar Covariance:* Under any given  $\mathbf{t}$ ,  $\Phi$ , we define  $\mathbf{W}_c = \mathbf{w}_c \mathbf{w}_c^H$ ,  $\mathbf{W}_c \geq \mathbf{0}$  and  $\text{rank}(\mathbf{W}_c) = 1$ , as well as  $\hat{\mathbf{H}}_e = \mathbf{h}_e \mathbf{h}_e^H$  and  $\hat{\mathbf{H}}_b = \mathbf{h}_b \mathbf{h}_b^H$ . Thus, it has

$$R_b(\mathbf{w}_c, \mathbf{R}_r) = \log_2 \left( 1 + \frac{\text{tr}(\hat{\mathbf{H}}_b \mathbf{W}_c)}{\text{tr}(\hat{\mathbf{H}}_b \mathbf{R}_r) + \sigma^2} \right), \quad (15)$$

$$R_e(\mathbf{w}_c, \mathbf{R}_r) = \log_2 \left( 1 + \frac{\text{tr}(\hat{\mathbf{H}}_e \mathbf{W}_c)}{\text{tr}(\hat{\mathbf{H}}_e \mathbf{R}_r) + \sigma^2} \right), \quad (16)$$

$$\begin{aligned}
 \mathcal{P}(\mathbf{w}_c, \mathbf{R}_r, \Phi) &= \mathbf{h}_e^H (\mathbf{w}_c \mathbf{w}_c^H + \mathbf{R}_r) \mathbf{h}_e \\
 &= \text{Tr}(\hat{\mathbf{H}}_e (\mathbf{W}_c + \mathbf{R}_r)). \quad (17)
 \end{aligned}$$

Hence, problem (P2) can be equivalently reformulated as

$$\begin{aligned}
 \text{(P2.1)} : \quad & \max_{\mathbf{w}_c, \mathbf{R}_r} R_b(\mathbf{w}_c, \mathbf{R}_r) - R_e(\mathbf{w}_c, \mathbf{R}_r) \\
 \text{s.t.} \quad & \text{tr}(\hat{\mathbf{H}}_e (\mathbf{W}_c + \mathbf{R}_r)) \geq \varepsilon, \quad (18a) \\
 & \text{tr}(\mathbf{W}_c) + \text{tr}(\mathbf{R}_r) \leq P_{\max}, \quad (18b) \\
 & \mathbf{R}_r \geq \mathbf{0}, \mathbf{W}_c \geq \mathbf{0}, \quad (18c) \\
 & \text{rank}(\mathbf{W}_c) = 1. \quad (18d)
 \end{aligned}$$

Note that problem (P2.1) is still non-convex due to the non-convex objective term. To deal with it, we recast the function  $R_b(\mathbf{W}_c, \mathbf{R}_r)$  in a form of difference of convex functions, i.e.,

$$R_b(\mathbf{W}_c, \mathbf{R}_r) = F_1(\mathbf{W}_c, \mathbf{R}_r) - F_2(\mathbf{R}_r), \quad (19)$$

where

$$F_1(\mathbf{W}_c, \mathbf{R}_r) = \log_2 \left( \sigma^2 + \text{tr}(\hat{\mathbf{H}}_b (\mathbf{W}_c + \mathbf{R}_r)) \right), \quad (20)$$

$$F_2(\mathbf{R}_r) = \log_2 \left( \sigma^2 + \text{tr}(\hat{\mathbf{H}}_b \mathbf{R}_r) \right). \quad (21)$$

Similarly, we rewrite the eavesdropping rate as

$$R_e(\mathbf{W}_c, \mathbf{R}_r) = f_1(\mathbf{W}_c, \mathbf{R}_r) - f_2(\mathbf{R}_r), \quad (22)$$

where

$$f_1(\mathbf{W}_c, \mathbf{R}_r) = \log_2 \left( \sigma^2 + \text{Tr}(\hat{\mathbf{H}}_e (\mathbf{W}_c + \mathbf{R}_r)) \right), \quad (23)$$

and

$$f_2(\mathbf{R}_r) = \log_2 \left( \sigma^2 + \text{Tr}(\hat{\mathbf{H}}_e \mathbf{R}_r) \right). \quad (24)$$

Due to the non-convexity of the objective function, we could adopt the SCA technique, combine it with the classical majorization-minimization (MM) algorithm, find a concave surrogate function for the objective function, and solve the problem alternately using this surrogate function. Specifically, the SCA takes advantage of the ease of solving convex optimization problems, transforms non-convex problems into a series of convex subproblems, and obtains an approximated solution to the original problem by alternately solving these subproblems. Hence, taking the first-order Taylor expansion on the concave function  $F_2(\mathbf{R}_r)$  and  $f_1(\mathbf{W}_c, \mathbf{R}_r)$ , we have

$$\begin{aligned}
 F_2(\mathbf{R}_r) &\leq F_2(\mathbf{R}_r^{(k_1)}) + \text{tr} \left( \frac{1}{\ln 2} \frac{\hat{\mathbf{H}}_b (\mathbf{R}_r - \mathbf{R}_r^{(k_1)})}{\sigma^2 + \text{Tr}(\hat{\mathbf{H}}_b \mathbf{R}_r^{(k_1)})} \right) \\
 &\triangleq \bar{F}_2(\mathbf{R}_r), \quad (25)
 \end{aligned}$$

and

$$\begin{aligned}
 f_1(\mathbf{W}_c, \mathbf{R}_r) &\leq f_1(\mathbf{W}_c^{(k_1)}, \mathbf{R}_r^{(k_1)}) \\
 &\quad + \text{Tr} \left( \nabla_{\mathbf{W}_c}^H f_1(\mathbf{W}_c^{(k_1)}, \mathbf{R}_r^{(k_1)}) (\mathbf{W}_c - \mathbf{W}_c^{(k_1)}) \right) \\
 &\quad + \text{Tr} \left( \nabla_{\mathbf{R}_r}^H f_1(\mathbf{W}_c^{(k_1)}, \mathbf{R}_r^{(k_1)}) (\mathbf{R}_r - \mathbf{R}_r^{(k_1)}) \right) \\
 &\triangleq \bar{f}_1(\mathbf{W}_c, \mathbf{R}_r), \quad (26)
 \end{aligned}$$

where  $\mathbf{W}_c^{(k_1)}$  and  $\mathbf{R}_r^{(k_1)}$  is the value of  $\mathbf{W}_c$  and  $\mathbf{R}_r$  in the  $k_1$ -th iteration, and

$$\begin{aligned}
 \nabla_{\mathbf{W}_c}^H f_1(\mathbf{W}_c^{(k_1)}, \mathbf{R}_r^{(k_1)}) &= \nabla_{\mathbf{R}_r}^H f_1(\mathbf{W}_c^{(k_1)}, \mathbf{R}_r^{(k_1)}) \\
 &= \frac{1}{\ln 2} \frac{\hat{\mathbf{H}}_e}{\sigma^2 + \text{Tr}(\hat{\mathbf{H}}_e \mathbf{W}_c^{(k_1)} + \text{Tr}(\hat{\mathbf{H}}_e \mathbf{R}_r^{(k_1)})}. \quad (27)
 \end{aligned}$$

Utilizing (25) and (26), construct a lower bound function for the objective function of problem (P2.1), and serve it as the surrogate function. Consequently, problem (P2.1) can be approximated as

$$\begin{aligned}
 \text{(P2.2)} \quad & \max_{\mathbf{W}_c, \mathbf{R}_r} F_1(\mathbf{W}_c, \mathbf{R}_r) - \bar{F}_2(\mathbf{R}_r) \\
 & \quad - \bar{f}_1(\mathbf{W}_c, \mathbf{R}_r) + f_2(\mathbf{R}_r) \\
 \text{s.t.} \quad & (18a), (18b), (18c), (18d).
 \end{aligned}$$

Using the SDR method to remove the rank constraint (18d), the transmit beamforming subproblem can be transformed as

$$(P2.3) \max_{\mathbf{W}_c, \mathbf{R}_r} F_1(\mathbf{W}_c, \mathbf{R}_r) - \bar{F}_2(\mathbf{R}_r) - \bar{f}_1(\mathbf{W}_c, \mathbf{R}_r) + f_2(\mathbf{R}_r) \\ \text{s.t.} \quad (18a), (18b), (18c),$$

which is a convex problem and can be addressed by CVX. Let  $\mathbf{W}_c^*$  and  $\mathbf{R}_r^*$  represent the optimal solution obtained to problem (P2.3). However, due to the lack of the rank-one constraint, the obtained solution may not be optimal to problem (P2.2). Therefore, according to [66], it is necessary to construct a solution that satisfies the rank-one constraint, as given in the following lemma.

**Lemma 1.** *Given the optimal solution  $\mathbf{W}_c^*$  and  $\mathbf{R}_r^*$  to problem (P2.3), the optimal solution to problem (P2.2) is*

$$\mathbf{w}_c^{opt} = (\mathbf{h}_e^H \mathbf{W}_c^* \mathbf{h}_e)^{-1/2} \mathbf{W}_c^* \mathbf{h}_e, \quad (28)$$

$$\mathbf{R}_r^{opt} = \mathbf{R}_r^* + \mathbf{W}_c^* - \mathbf{w}_c^{opt} (\mathbf{w}_c^{opt})^H. \quad (29)$$

*Proof.* Define  $\mathbf{W}_c^{opt} = \mathbf{w}_c^{opt} (\mathbf{w}_c^{opt})^H \succeq 0$  (of rank one), and  $\mathbf{R}_r^{opt}$  are the optimal solutions to problem (P2.1). According to (29),  $\mathbf{W}_c^{opt} + \mathbf{R}_r^{opt} = \mathbf{W}_c^* + \mathbf{R}_r^*$ . Thus, it satisfies the power constraint of the objective. It is not difficult to prove  $\text{tr}(\hat{\mathbf{H}}_e(\mathbf{W}_c^{opt} + \mathbf{R}_r^{opt})) = \text{tr}(\hat{\mathbf{H}}_e(\mathbf{W}_c^* + \mathbf{R}_r^*))$ , so it meets the sensing performance index of the objective. Therefore, it completes the proof.  $\square$

The detailed algorithm for solving  $\mathbf{w}_c$  and  $\mathbf{R}_r$  is summarized in Algorithm 1. Here,  $\epsilon_1$  represents the precision of convergence. In the initialization phase, the maximum transmission criterion (MRT) is adopted. The phase shift matrix  $\Phi^{(0)}$  is set as an identity matrix. On this basis, in accordance with the MRT criterion and following the principle that the beam direction is consistent with the equivalent channel direction, the beamforming vector is precisely aligned with the user and target directions. Through this method, the useful signal can be maximally enhanced in the initial state, thereby obtaining the parameters  $\mathbf{w}_c^{(0)}$  and  $\mathbf{R}_r^{(0)}$  in the initial state.

2) *Optimization of Phase Shift of IRS:* With the acquired  $\mathbf{w}_c$  and  $\mathbf{R}_r$  according to Algorithm 1, we define  $\mathbf{v} = (e^{j\vartheta_1}, e^{j\vartheta_2}, \dots, e^{j\vartheta_N})^H$ . Then, we introduce the following relationships. First, consider  $\zeta_i^H \mathbf{w}_c = \mathbf{v} \text{diag}(\zeta_i^H) \mathbf{H}(\mathbf{t})^H \mathbf{w}_c$ , where  $i \in (b, e)$ . By introducing  $\mathbf{V} = \mathbf{v} \mathbf{v}^H$ , we can obtain  $|\zeta_i^H \mathbf{w}_c|^2 \triangleq \text{Tr}(\hat{\mathbf{A}}_i \mathbf{V})$ . Here,  $\hat{\mathbf{A}}_i = \text{diag}(\zeta_i^H) \mathbf{H}^H \mathbf{w}_c \mathbf{w}_c^H \mathbf{H} \text{diag}(\zeta_i)$  and  $i \in (b, e)$ . Similarly, for  $\zeta_i^H \mathbf{R}_r \zeta_i$ , we have  $\zeta_i^H \mathbf{R}_r \zeta_i = \text{Tr}(\hat{\mathbf{N}}_i \mathbf{V})$ , with  $\hat{\mathbf{N}}_i = \text{diag}(\zeta_i^H) \mathbf{H}^H \mathbf{R}_r \mathbf{H} \text{diag}(\zeta_i)$  and  $i \in (b, e)$ . Thus, the optimization problem can be expressed as follows

**Algorithm 1:** SCA-based algorithm for solving problem (P2.1)

**Input:**  $\{\mathbf{w}_c^{(0)}, \mathbf{R}_r^{(0)}\}$ .  
**1 Initialize**  $\Delta = \infty, k_1 = 0$ ;  
**2 While** ( $\Delta \geq \epsilon_1$ )  
**3 At the  $k_1$ -th iteration, solve the non-convex problem (P2.3) and get  $\mathbf{W}_c^*$  and  $\mathbf{R}_r^*$ ;**  
**4 Construct  $\mathbf{w}_c^{opt}$  and  $\mathbf{R}_r^{opt}$  using equations (28) and (29) for the  $(k_1+1)$ -th iteration to get  $\mathbf{W}_c^{(k_1+1)}$  and  $\mathbf{R}_r^{(k_1+1)}$ ;**  
**5 Calculate  $R_{sec}^{(k_1+1)}$  based on  $\mathbf{w}_c^{opt}$  and  $\mathbf{R}_r^{opt}$ ;**  
**6 Update**  
**7  $\Delta = |R_{sec}^{(k_1+1)} - R_{sec}^{(k_1)}|, R_{sec}^{(k_1)} \leftarrow R_{sec}^{(k_1+1)}$ ;**  
**8  $\mathbf{w}_c^{k_1} = \mathbf{w}_c^{opt}, \mathbf{R}_r^{k_1} = \mathbf{R}_r^{opt}, k_1 = k_1 + 1$ ;**  
**9 End while**  
**Output:**  $\{\mathbf{w}_c^{opt}, \mathbf{R}_r^{opt}\}$ .

$$(P2.4) : \max_{\mathbf{V}} \log_2(1 + \frac{\text{Tr}(\hat{\mathbf{A}}_b \mathbf{V})}{\text{Tr}(\hat{\mathbf{N}}_b \mathbf{V}) + \sigma^2}) - \log_2(1 + \frac{\text{Tr}(\hat{\mathbf{A}}_e \mathbf{V})}{\text{Tr}(\hat{\mathbf{N}}_e \mathbf{V}) + \sigma^2}) \\ \text{s.t.} \quad \text{Tr}(\hat{\mathbf{N}}_e \mathbf{V}) \geq \varepsilon, \quad (30a) \\ \mathbf{V} \succeq 0, \quad (30b) \\ \text{rank}(\mathbf{V}) = 1, \quad (30c) \\ [\mathbf{V}]_{n,n} = 1, n \in \mathcal{N}. \quad (30d)$$

According to the properties of logarithms, the objective function can be transformed into

$$R_{sec}(\mathbf{V}) = \log_2(\sigma^2 + \text{Tr}(\hat{\mathbf{N}}_b \mathbf{V}) + \text{Tr}(\hat{\mathbf{A}}_b \mathbf{V})) - \underbrace{\log_2(\sigma^2 + \text{Tr}(\hat{\mathbf{N}}_b \mathbf{V}))}_{I_1(\mathbf{V})} - \underbrace{\log_2(\sigma^2 + \text{tr}(\hat{\mathbf{A}}_e \mathbf{V}) + \text{tr}(\hat{\mathbf{N}}_e \mathbf{V}))}_{I_2(\mathbf{V})} + \log_2(\sigma^2 + \text{Tr}(\hat{\mathbf{N}}_e \mathbf{V})). \quad (31)$$

By leveraging the SCA approach to approximate its convexity, we check its first-order Taylor expansion on  $I_1$  and  $I_2$  to obtain their upper bounds, which can be expressed as

$$I_1(\mathbf{V}) \leq \log_2(\sigma^2 + \text{tr}(\hat{\mathbf{N}}_b \mathbf{V}^{(k_2)})) + \text{Tr}(\frac{1}{\ln 2} \frac{\hat{\mathbf{N}}_b}{\sigma^2 + \text{tr}(\hat{\mathbf{N}}_b \mathbf{V}^{(k_2)})} (\mathbf{V} - \mathbf{V}^{(k_2)})), \quad (32)$$

and

$$I_2(\mathbf{V}) \leq \log_2(\sigma^2 + \text{tr}(\hat{\mathbf{A}}_e \mathbf{V}^{(k_2)}) + \text{tr}(\hat{\mathbf{N}}_e \mathbf{V}^{(k_2)})) + \text{Tr}(\frac{1}{\ln 2} \frac{\hat{\mathbf{N}}_e + \hat{\mathbf{A}}_e}{\sigma^2 + \text{tr}(\hat{\mathbf{N}}_e \mathbf{V}^{(k_2)}) + \text{tr}(\hat{\mathbf{A}}_e \mathbf{V}^{(k_2)})} (\mathbf{V} - \mathbf{V}^{(k_2)})), \quad (33)$$



where  $\mathbf{V}^{(k_2)}$  is the locally optimal solution  $\mathbf{V}$  at the  $k_2$ -th iteration. Substituting the upper bounds of  $I_1(\mathbf{V})$  and  $I_2(\mathbf{V})$  in (32) and (33) and omitting the constant terms in (31), problem (P2.4) can be reformulated as follows

$$(P2.5) : \max_{\mathbf{V}} \log_2 \left( \sigma^2 + \text{Tr}(\hat{\mathbf{N}}_b \mathbf{V}) + \text{Tr}(\hat{\mathbf{A}}_b \mathbf{V}) \right) \\ - \text{Tr} \left( \frac{1}{\ln 2} \frac{\hat{\mathbf{N}}_b \mathbf{V}}{\sigma^2 + \text{tr}(\hat{\mathbf{N}}_b \mathbf{V}^{(k_2)})} \right) \\ - \text{Tr} \left( \frac{1}{\ln 2} \frac{\hat{\mathbf{N}}_e + \hat{\mathbf{A}}_e}{\sigma^2 + \text{tr}(\hat{\mathbf{N}}_e \mathbf{V}^{(k_2)}) + \text{tr}(\hat{\mathbf{A}}_e \mathbf{V}^{(k_2)})} \mathbf{V} \right) \\ + \log_2 \left( \sigma^2 + \text{Tr}(\hat{\mathbf{N}}_e \mathbf{V}) \right) \\ \text{s.t.} \quad (30a), (30b), (30c), (30d).$$

It can be observed that the convex problem can be effectively solved by relaxing the constraint  $\text{rank}(\mathbf{V}) = 1$  in (30c). The SDR and Gaussian randomization algorithm can be used to obtain an approximate solution for  $\mathbf{v}$ , but it cannot guarantee the convergence of the overall algorithm. SRCR diverges from traditional algorithms, which entirely abandon the rank-one constraint. Instead, it adjusts the constraint condition through the relaxation parameter  $\varpi \in [0, 1]$ . When  $\varpi = 0$ , it's tantamount to discarding the rank-one constraint, allowing for the discovery of a feasible point. As  $\varpi$  steadily rises from 0, the rank-one constraint is progressively met until it eventually nears the true rank-one constraint set. Therefore, according to [67], SRCR is adopted to equivalently transform (30c) into

$$\mathbf{u}_{\max}^H(\mathbf{V}^{(k_2)}) \mathbf{V} \mathbf{u}_{\max}(\mathbf{V}^{(k_2)}) \geq \varpi^{(k_2)} \text{Tr}(\mathbf{V}), \quad (34)$$

where  $\mathbf{V}^{(k_2)}$  represents a feasible solution obtained at the  $k_2$ -th iteration. The eigenvector corresponding to the largest eigenvalue of  $\mathbf{V}^{(k_2)}$  is denoted as  $\mathbf{u}_{\max}(\mathbf{V}^{(k_2)})$ . Additionally, we sequentially increase  $\varpi^{(k_2)}$  from 0 to 1 through iterations in order to gradually approach a rank-one solution. After each iteration, the relaxation parameter can be updated as

$$\varpi^{(k_2+1)} \leftarrow \min \left( 1, \frac{\chi_{\max}(\mathbf{V}^{(k_2+1)})}{\text{tr}(\mathbf{V}^{(k_2+1)})} + \varrho^{(k_2+1)} \right), \quad (35)$$

where  $\chi_{\max}(\mathbf{V}^{(k_2+1)})$  represents the largest eigenvalue of  $\mathbf{V}^{(k_2+1)}$  and  $\varrho^{(k_2+1)}$  denotes the step size for the weight parameter updating. The optimization problem can then be expressed

$$(P2.6) : \max_{\mathbf{V}} \log_2 \left( \sigma^2 + \text{Tr}(\hat{\mathbf{N}}_b \mathbf{V}) + \text{Tr}(\hat{\mathbf{A}}_b \mathbf{V}) \right) \\ - \text{Tr} \left( \frac{1}{\ln 2} \frac{\hat{\mathbf{N}}_b \mathbf{V}}{\sigma^2 + \text{tr}(\hat{\mathbf{N}}_b \mathbf{V}^{(k_2)})} \right) \\ - \text{Tr} \left( \frac{1}{\ln 2} \frac{(\hat{\mathbf{N}}_e + \hat{\mathbf{A}}_e) \mathbf{V}}{\sigma^2 + \text{tr}(\hat{\mathbf{N}}_e \mathbf{V}^{(k_2)}) + \text{tr}(\hat{\mathbf{A}}_e \mathbf{V}^{(k_2)})} \right) \\ + \log_2 \left( \sigma^2 + \text{Tr}(\hat{\mathbf{N}}_e \mathbf{V}) \right) \\ \text{s.t.} \quad (30a), (30b), (30d), (34).$$

Problem (P2.6) can be solved by the CVX tool. Similarly, the detailed algorithm steps for optimizing  $\mathbf{V}$  by using the SCA algorithm will be described in Algorithm 2.

Here,  $\epsilon_2$  represents the predefined threshold and when  $\Delta_2 = \text{Tr}(\mathbf{V}^{(k_2)}) / \chi_{\max}(\mathbf{V}^{(k_2)})$  is less than  $\epsilon_2$ , the objective value of problem (P2.6) converges. After calculating matrix  $\mathbf{V}^*$  according to Algorithm 2, find the eigenvector  $\mathbf{e}^{\text{opt}}$  corresponding to its maximum eigenvalue. Then  $\Phi$  is the diagonal matrix formed with  $\mathbf{e}^{\text{opt}}$  as its diagonal elements.

---

**Algorithm 2:** SCA-based algorithm for solving problem (P2.4)

---

**Input:**  $\{\mathbf{w}_c^{\text{opt}}, \mathbf{R}_r^{\text{opt}}\}$ .

- 1 **Initialize** a feasible iteration point  $\{\mathbf{V}^{(0)}, \varrho^{(0)}\}$ . Set  $\Delta_2 = \infty$ ,  $\varpi^{(0)} = 0$ ,  $k_2 = 0$ ;
- 2 **While** ( $\Delta_2 \geq \epsilon_2$ )
- 3 **Solve** non-convex problem (P2.6) with  $\{\varpi^{(k_2)}, \mathbf{V}^{(k_2)}\}$  to obtain  $\mathbf{V}^*$ ;
- 4 **IF** (problem (P2.6) is solvable)
- 5 **Update**  $\mathbf{V}^{(k_2+1)} = \mathbf{V}^*$ ,  $\varrho^{(k_2+1)} = \varrho^{(0)}$ ;
- 6 **Else**
- 7 **Update**  $\mathbf{V}^{(k_2+1)} = \mathbf{V}^{(k_2)}$ ,  $\varrho^{(k_2+1)} = \frac{\varrho^{(k_2)}}{2}$ ;
- 8 **End**
- 9 **Update**  $\varpi^{(k_2+1)}$  by (35) and  $k_2 = k_2 + 1$ ;
- 10 **Calculate**  $\Delta_2 = \frac{\text{Tr}(\mathbf{V}^{(k_2+1)})}{\chi_{\max}(\mathbf{V}^{(k_2+1)})}$ ;
- 11 **End while**

---

### B. Optimization of Antenna Position

With the obtained  $\mathbf{w}_c$ ,  $\mathbf{R}_r$  and  $\Phi$ , we next optimize the antenna position  $\mathbf{t}$  and the objective  $R_{\text{sec}}(\mathbf{w}_c, \mathbf{R}_r, \Phi, \mathbf{t})$  is reduced as  $R_{\text{sec}}(\mathbf{t})$  are calculated according to the given antenna positions. Thus, the original problem (P1) can be transformed to the following optimization problem

$$(P3) : \max_{\mathbf{t}} R_{\text{sec}}(\mathbf{t}) \\ \text{s.t.} \quad \mathbf{h}_{r,e}^H \Phi \mathbf{H}(\mathbf{t})^H (\mathbf{w}_c \mathbf{w}_c^H + \mathbf{R}_r) \mathbf{H}(\mathbf{t}) \Phi \mathbf{h}_{r,e} \geq \varepsilon, \quad (36a) \\ |t_i - t_j| \geq d_{\min}, \forall i, j \in \mathcal{M}, i \neq j, \quad (36b) \\ t_m \in [0, J], \forall m \in \mathcal{M}. \quad (36c)$$

Note that the high non-convexity of the above problem makes it challenging to solve. Moreover, the high-dimensional transmit response matrix of the moving antennas significantly increases the complexity of the problem when using search-based methods. Therefore, the problem can be solved by using the PSO algorithm.

specifically, the principle of the PSO lies in representing each potential solution within the solution space by a particle. These particles fly at a certain speed. During flight, they adjust their positions continuously based on their respective personal best positions and the global best position found by the entire particle swarm, constantly searching for the global optimal solution. We first introduce  $S$  particles and initialize their positions and velocities to  $\mathbf{P} = \{\mathbf{p}_1^{(0)}, \mathbf{p}_1^{(0)}, \dots, \mathbf{p}_S^{(0)}\}$  and  $\mathbf{U} = \{\boldsymbol{\mu}_1^{(0)}, \boldsymbol{\mu}_2^{(0)}, \dots, \boldsymbol{\mu}_S^{(0)}\}$  respectively, where  $\boldsymbol{\mu}_s^{(0)}$  represents the initial velocity of particle  $s$  and each particle represents a possible solution for antenna position, i.e.,

$$\mathbf{p}_s^{(0)} = [t_{s,1}^{(0)}, t_{s,2}^{(0)}, \dots, t_{s,M}^{(0)}], \quad (36)$$



where  $0 \leq t_{s,k}^{(0)} \leq J$  for  $1 \leq k \leq M, 1 \leq k \leq S$ , which represents the possible position of the  $k$ -th antenna of the  $s$ -th particle within the finite movement region. The PSO algorithm could efficiently search for the optimal particle among these  $S$  particles and identify it as the solution to problem (P3). The detailed process is outlined as follows

a) *Definition of the Fitness Function:* The fitness function is used to evaluate the performance of each particle, which means to determine whether the particle's position can achieve the desired performance requirements. Considering constraints (13a) and (13e), we introduce a penalty function as

$$\mathcal{I}(\mathbf{p}_s^{(q)}) = \tau_t \sum_{a=1}^{M-1} \sum_{\tilde{a}=a+1}^M \delta\left(\left|t_a^{(q)} - t_{\tilde{a}}^{(q)}\right| < d_{\min}\right) + \tau_r \delta\left(\mathcal{P}(\mathbf{p}_s^{(q)}) < \epsilon\right), \forall s \in [1, S], \quad (37)$$

where  $\mathbf{p}_s^{(q)}$  is the antenna position of the  $s$ -th particle in the  $q$ -th ( $1 \leq q \leq Q$ ) iteration, and  $Q$  denotes the maximum number of iterations.  $\tau_t$  and  $\tau_r$  represent the penalty factors for the antenna position constraint (13e) and the sensing constraint (13a), respectively. They can adjust the severity of the penalties.  $\delta(\cdot)$  is an indicator function, which equals 1 when the condition is satisfied and 0 otherwise. Thus, the fitness function is defined as

$$\mathcal{F}(\mathbf{p}_s^{(q)}) = R_{\text{sec}}(\mathbf{p}_s^{(q)}) - \mathcal{I}(\mathbf{p}_s^{(q)}). \quad (38)$$

At the same time,  $\tau_t$  and  $\tau_r$  need to use the penalty function at position  $R_{\text{sec}}(\mathbf{p}_s^{(q)}) - (\tau_t + \tau_r) < 0$  to drive the particles to satisfy the relevant constraints. Therefore, as the number of iterations increases, the penalty function  $\mathcal{I}(\mathbf{p}_s^{(q)})$  will converge to 0.

b) *Updating of the Particles' Positions and Velocities:* The position of the  $s$ -th particle is controlled by its own local best position  $\mathbf{p}_s^*$  and the global best position  $\mathbf{p}^*$  among all particles, which is evaluated by the fitness function. Therefore, according to [68], the position and velocity update of the  $s$ -th particle can be expressed as

$$\mathbf{v}_s^{(q+1)} = \varsigma \mathbf{v}_s^{(q)} + c_1 r_2 (\mathbf{p}_s^* - \mathbf{p}_s^{(q)}) + c_2 r_3 (\mathbf{p}^* - \mathbf{p}_s^{(q)}), \quad (39)$$

$$\mathbf{p}_s^{(q+1)} = \mathcal{B}(\mathbf{p}_s^{(q)} + \mathbf{v}_s^{(q+1)}), \quad (40)$$

where  $c_1$  and  $c_2$  are individual and global learning factors, respectively, for determining the step size of each particle moving towards the best position;  $r_2$  and  $r_3$  are two random parameters uniformly distributed in  $[0,1]$ , which aim to increase the randomness of the search for escaping from local optima;  $\varsigma$  represents the inertia weight, to balances the particle's search speed and accuracy [68], its value will gradually decrease as the number of iterations increases, which is shown as

$$\varsigma = \left( \varsigma_{\max} - \frac{(\varsigma_{\max} - \varsigma_{\min})}{Q} q \right), \quad (41)$$

where  $\varsigma_{\max}$  and  $\varsigma_{\min}$  are the maximum and minimum value of  $\varsigma$ .

Since the antenna position cannot exceed the movement range, namely constraint (13f), the coordinates of points that

exceed the range are mapped to the corresponding maximum/minimum values,

$$[\mathcal{B}(\tilde{\mathbf{p}})]_i = \begin{cases} 0, & \text{if } [\tilde{\mathbf{p}}]_i < 0, \\ J, & \text{if } [\tilde{\mathbf{p}}]_i > J, \\ [\tilde{\mathbf{p}}]_i, & \text{otherwise.} \end{cases} \quad (42)$$

Therefore, according to the mapping function  $\mathcal{B}(\tilde{\mathbf{p}})$ , it ensures that the antenna position remains within the feasible region throughout the iteration process.

### C. Overall Solution

The overall algorithm framework proceeds as follows: Initially,  $S$  particles are initialized with randomized positions and velocities under predefined system constraints. For each particle's antenna configuration, the variables of transmit beamforming  $\mathbf{w}_c$ , sensing covariance matrix  $\mathbf{R}_r$  and IRS phase shifts  $\Phi$  are iteratively optimized via Algorithm 1 and Algorithm 2, with the corresponding secure rate  $R_{\text{sec}}$  serving as the fitness metric. Following this, local best positions  $\mathbf{p}_s^*$  and the global best  $\mathbf{p}^*$  are updated through fitness comparisons. During  $Q$  iterations, the inertia weight  $\varsigma$  is dynamically scaled, after which velocity and position vectors are refreshed using PSO kinematic rules. Each update triggers re-evaluation of  $R_{\text{sec}}$ ,  $\mathbf{p}_s^*$  and  $\mathbf{p}^*$ . Upon convergence, the optimal antenna configuration  $\mathbf{t}$  is derived from  $\mathbf{p}^*$ , yielding the joint solutions  $\mathbf{w}_c$ ,  $\mathbf{R}_r$  and  $\Phi$  that satisfy all security and sensing constraints. The overall algorithm details for solving problem (P1) will be summarized in Algorithm 3.

## IV. NUMERICAL RESULTS

In this section, we present numerical simulation results to demonstrate the performance of the algorithm. We consider the distance-dependent path loss model, that is,  $\beta = \beta_0(d/d_0)^{-\bar{\alpha}}$ , where  $\beta_0 = -30$  dB represents the path loss at the reference distance of  $d_0 = 1$  m, and we set  $\bar{\alpha}$  as 2.2. Throughout the simulation, we set the partitions of the BS and IRS as (0m, 0m), (0m, 50m). The user and target are placed 2m away from the IRS, with the azimuth angles of both the user and the target relative to the IRS set to  $\pi/6$  and  $-\pi/6$ . Additionally, some parameters are carefully defined in Table II.

It is observed from Fig. 2 (a), regardless of how the parameters are set, the algorithm proposed can achieve convergence in a consistent way. Further observation reveals that when other parameters remain unchanged, there are obvious correlations between the secure rate and the number of antennas, the number of IRS, the movement range of antennas, and the sensing threshold. Specifically, as the number of antennas increases, the secure rate may increase accordingly; changes in the number of IRS also have an impact on the secure rate; the size of the antenna movement range affects the change of the secure rate to a certain extent; and the adjustment of the sensing threshold also shows a certain correlation with the secure rate.

Figure 2 (b) performs a comparative analysis of the performance between the FPA and the MA. The results show that the performance of both can gradually converge as the

**Algorithm 3:** PSO-based algorithm for solving problem (P1)

**Input:**  $N, M, J, \sigma^2, \epsilon_1, \epsilon_2, d_r, \epsilon, d_{\min}, P_{\max}, Q, \varsigma_{\max}, \varsigma_{\min}, c_1, c_2, \tau_t, \tau_r, \{\theta_{m,l}\}, \{\rho_r^l(\mathbf{r}_n)\}$ .

- 1 **Initialize** the velocity  $\mathbf{U}^{(0)}$  and position  $\mathbf{P}^{(0)}$  of  $S$  particles;
- 2 **Based** on the initial positions of the particles, combined with Algorithm 1 and Algorithm 2, solve for the corresponding values of  $\mathbf{w}_c^{(0)}, \mathbf{R}_r^{(0)}, \mathbf{V}^{(0)}$ , and calculate  $R_{sec}^{(0)}$ . Set  $R_{sec}(\mathbf{p}_n^{(0)}) = R_{sec}^{(0)}$ , and then calculate the fitness value for each particle according to (38);
- 3 **Let** the local best position  $\mathbf{p}_s^* = \mathbf{p}_s^{(0)}$ , and the global best position  $\mathbf{p}^* = \arg \max_{\mathbf{p}_n^{(0)}} \{\mathcal{F}(\mathbf{p}_1^{(0)}), \mathcal{F}(\mathbf{p}_2^{(0)}), \dots, \mathcal{F}(\mathbf{p}_S^{(0)})\}$ ;
- 4 **For** ( $q = 1$  to  $Q$ )
  - 5 **Calculate**  $\varsigma$  according to (41);
  - 6 **For** ( $s = 1$  to  $S$ )
    - 7 **Update** the positions and velocities of the particles respectively according to (40) and (39);
    - 8 **Evaluate** the fitness function of particle  $s$  by combining with Algorithm 1 and Algorithm 2, and then update it;
    - 9 **If** ( $\mathcal{F}(\mathbf{p}_s^{(q)}) > \mathcal{F}(\mathbf{p}_{s,best})$ )
      - 10 **Update**  $\mathbf{p}_{s,best} = \mathbf{p}_s^{(q)}$ ;
    - 11 **Else**
      - 12 **If** ( $\mathcal{F}(\mathbf{p}_s^{(q)}) > \mathcal{F}(\mathbf{p}_{best})$ )
        - 13 **Update**  $\mathbf{p}_{best} = \mathbf{p}_s^{(q)}$ ;
    - 14 **End**
  - 15 **End**
  - 16 **End**
  - 17 **Obtain**  $\mathbf{t} = \mathbf{p}_{best}$ ;
  - 18 **Calculate** the corresponding  $\mathbf{w}_c, \mathbf{R}_r$  and  $\Phi$  according to Algorithm 1 and Algorithm 2.

TABLE II: Simulation Parameters

Parameter	Description	Value
$M$	Number of antennas	4
$N$	Number of IRS elements	36
$J$	The length of the linear transmit array	$4\lambda$
$d_{\min}$	Minimum inter-MA distance	$\lambda/2$
$L$	Number of channel paths	10
$\rho_0$	Path loss at the reference distance	-30 dB
$\alpha$	Path loss exponent	2.2
$\sigma^2$	Average noise powers	-110 dBm
$P_{\max}$	Power of ISAC BS	10 dBm
$S$	Number of particles	100
$Q$	Maximum numbers of iterations	100
$\tau_t$	Penalty factors for antenna position	10
$\tau_r$	Penalty factors for sensing constraint	10
$c_1$	Personal learning factors	1.4
$c_2$	Global learning factors	1.4
$\epsilon_1$	Convergence thresholds for beamforming	$10^{-4}$
$\epsilon_2$	Convergence thresholds for $\Phi$	$10^{-4}$

number of iterations increases. However, compared to the FPA,

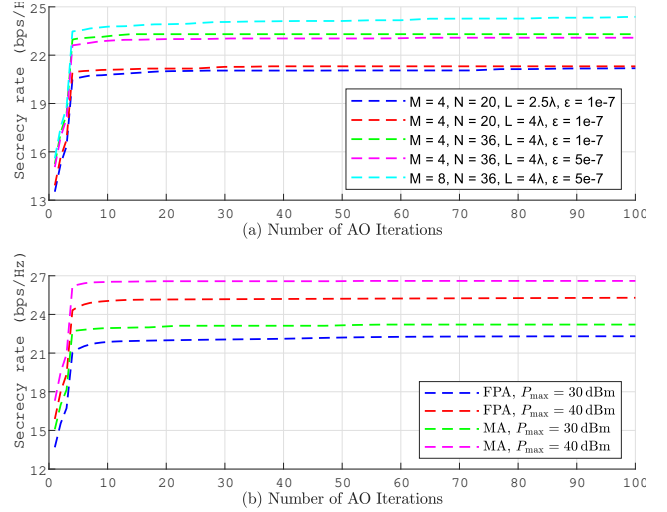


Fig. 2: Convergence performance of the proposed algorithm.

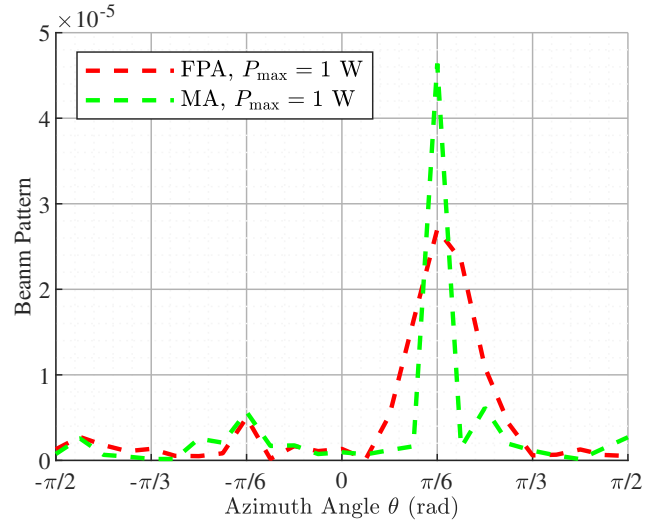


Fig. 3: Beam gain diagram.

the MA demonstrates significant advantages and can achieve a higher communication security rate. This result strongly proves the important role of the MA in channel reconstruction. It can better adapt to changes in the channel environment by flexible position adjustment, thereby enhancing the security and efficiency of communication.

Figure 3 clearly presents the beam gain of the signal. Through careful observation of this figure, it can be found that when certain specific conditions are met, the signal strength reaches its peak, which fully indicates that the signal power is maximized in the direction of the user. In the direction of the eavesdropping target, the signal also has a certain power. During the simulation, the sensing threshold is set at  $5 \mu\text{W}$ , and at this time, the signal strength can exactly reach this threshold level, which means that the minimum requirement for sensing performance is met. In short, this result shows that during the process of exploring the target, the goal of enabling the user to obtain the strongest energy has been successfully achieved. While ensuring the sensing performance, the signal power distribution in the user's direction has been optimized.

Three benchmark algorithms are introduced for comparison

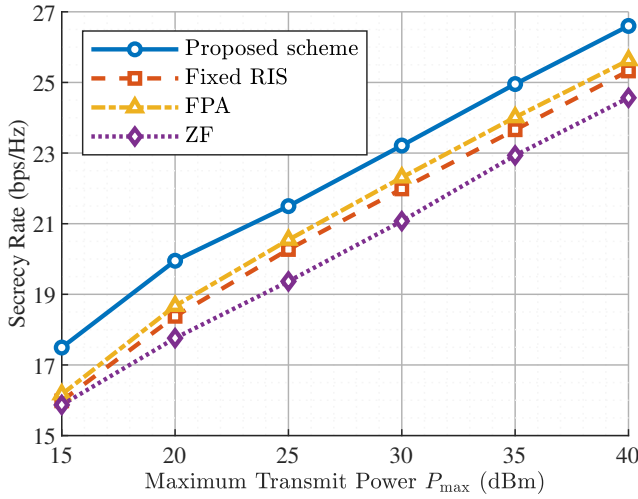


Fig. 4: Secure rate  $R_{sec}$  versus transmission power.

with the proposed algorithm.

- **FPA:** This ignores the optimization of antenna positions and selects a traditional fixed-position antenna array. It jointly optimizes the IRS phase shifts, communication beamforming, and the sensing covariance matrix.
- **Fixed IRS:** It indicates ignoring the optimization of IRS phase shifts, selecting fixed IRS phase shifts, and only optimizing the antenna positions, communication beamforming, and the sensing covariance matrix.
- **Zero-forcing (ZF):** Both communication beamforming and the sensing covariance are solved using ZF approach, and it jointly optimizes IRS phase shifts and antenna positions.

In Fig. 4, the inherent relationship between the transmit power and the secure rate is depicted. Through careful observation of the data in the figure, it can be found that as the transmit power gradually increases, the secure rate shows a clear linear growth trend. This phenomenon indicates that, in the current research context, an increase in transmit power can effectively drive an increase in the secure rate. Meanwhile, it is particularly noteworthy that the proposed scheme significantly outperforms the other three comparative schemes in terms of performance. Whether in the stage of lower transmit power or when the transmit power is relatively high, the secure rate corresponding to this scheme always remains at a higher level. This not only fully demonstrates the effectiveness and superiority of the scheme proposed in this paper but also further illustrates that the reasonable setting of various variables has a positive promoting effect on the improvement of the secure rate.

Fig. 5 mainly presents the relationship between the number of IRS reflection elements and the secure rate. It is not difficult to find from the figure that as the number of IRS reflection elements gradually increases, the security rate has been significantly improved, showing a favorable promoting trend. This clearly indicates that the IRS has a positive feedback effect on the performance of ISAC. More IRS reflection elements can optimize the signal propagation path and enhance the signal strength, thereby improving the system's secure rate, highlighting the key value of the IRS in improving the

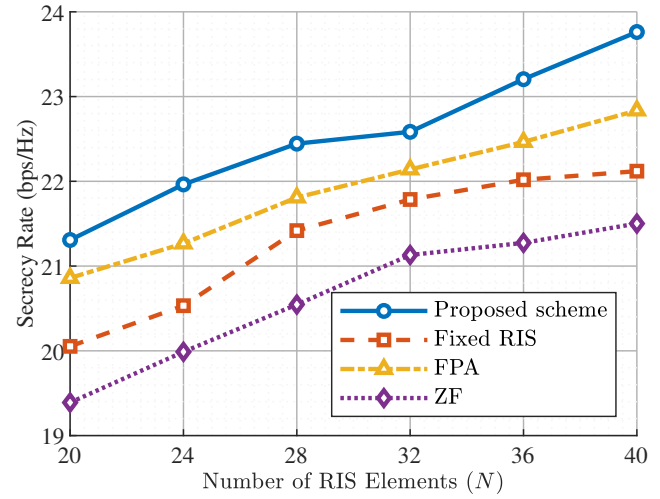


Fig. 5: Secure rate  $R_{sec}$  versus Number of IRS elements.

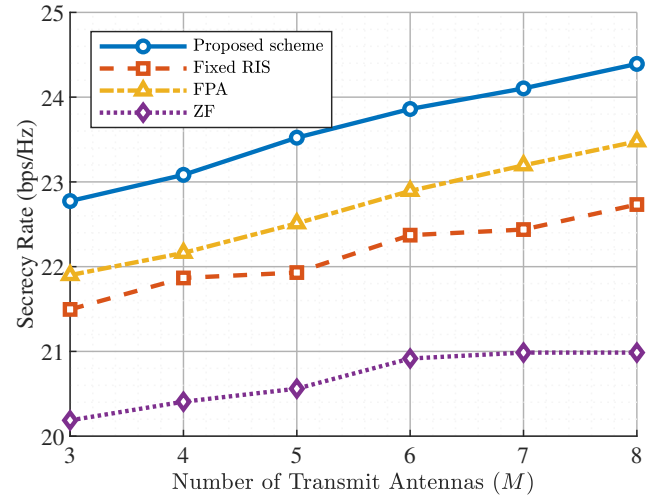


Fig. 6: Secure rate  $R_{sec}$  versus number of transmit antennas.

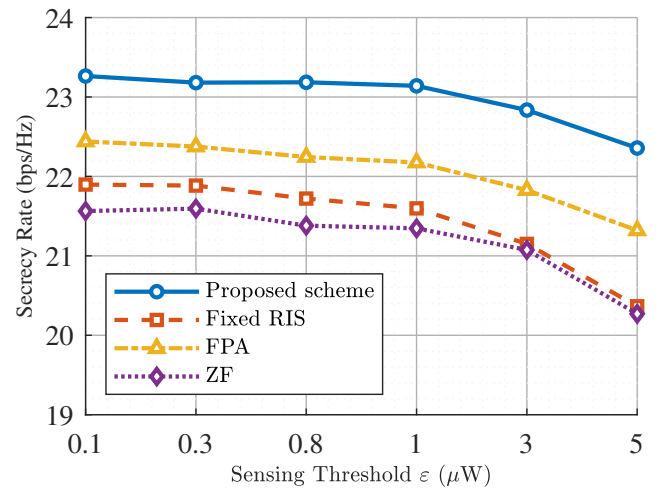


Fig. 7: Secure rate  $R_{sec}$  versus sensing beamforming gain.

performance of ISAC. It is worth noting that under the same conditions, the proposed algorithm could perform better in improving the secure rate compared with other benchmarking schemes.

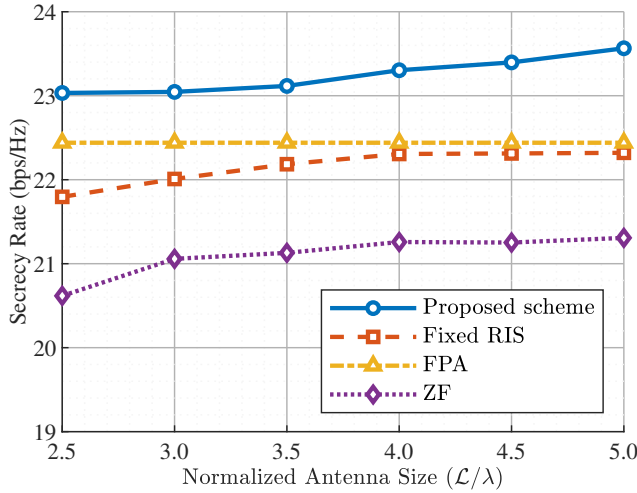


Fig. 8: Secure rate  $R_{sec}$  versus normalized antenna size.

Fig. 6 reveals the close relationship between the secure rate and the number of BS transmitting antennas. It can be intuitively and obviously observed from the figure that as the number of BS transmitting antennas gradually increases, the secure rate shows a significant upward trend and achieves a relatively large increase. This phenomenon fully demonstrates that expanding the scale of antennas has an extremely favorable promoting effect on improving the performance of wireless communication. It means that in a wireless communication system, increasing the number of BS transmitting antennas can effectively enhance the stability and efficiency of signal transmission, laying a solid foundation for the improvement of the secure rate.

Fig. 7 shows the impact of the sensing threshold on secure communication performance. As shown in the figure, as the sensing threshold increases, the security performance declines. At the sensing threshold of  $\varepsilon = 0.8\mu W$ , the proposed scheme outperforms the Fixed RIS by 0.28 dB, the FPA by 0.18 dB, and the ZF by 0.35 dB in secrecy rate, as clearly indicated by the visual annotations. This is mainly due to the trade-off between sensing and communication. When sensing performance improves (i.e., when more energy is directed towards eavesdropper detection), the signal strength available for legitimate users weakens. As the sensing performance constraints are further tightened, the security performance will drop sharply. This is because enhanced sensing performance leads to improved signal quality at the eavesdropping target, thereby exacerbating the degradation of security performance. Identifying the optimal trade-off between sensing and security remains a significant challenge.

Fig. 8 illustrates the relationship between the normalized antenna size ( $L/\lambda$ ) and the secrecy rate. Since the FPA antenna is a fixed antenna, its performance remains unaffected and stays as a straight line with the increase in the normalized size of the antenna. As the normalized antenna size increases, the proposed scheme can leverage more spatial channel information, leading to a continuous improvement in the secrecy rate. When the normalized antenna size reaches a certain level (e.g.,  $L/\lambda=4.0$ ), the secrecy rate tends to stabilize. When  $L/\lambda=5.0$ , the proposed scheme outperforms Fixed IRS by 0.24 dB, FPA by 0.21 dB, and ZF by 0.44 dB. This performance stabilization

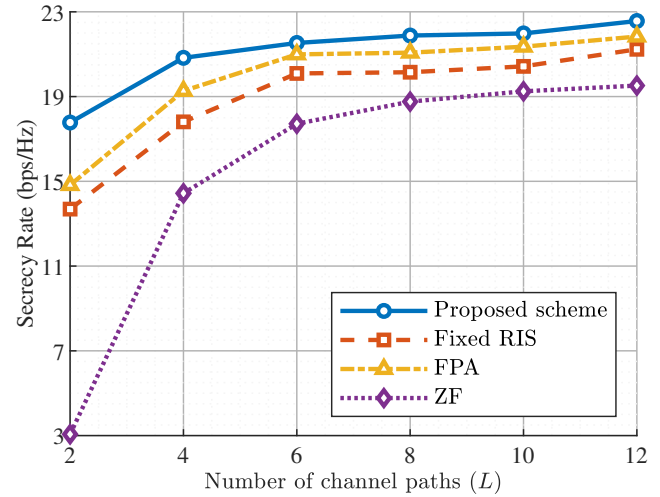


Fig. 9: Secure rate  $R_{sec}$  versus number of channel paths.

indicates that the antenna's influence on the secrecy rate has reached a saturation point: beyond this point, further increasing the antenna size will only result in diminishing performance gains.

Finally, the relationship between the number of channel paths ( $L$ ) and the secrecy rate is shown in Fig. 9. As the number of channel paths increases, the proposed scheme can leverage more diverse channel state information, leading to a continuous improvement in the secrecy rate. It can be observed from the figure that the ZF algorithm exhibits poor security performance when the number of paths is low. The main reason for this is that the rank of the channel matrix is lower than the number of transmit/receive antennas, which results in the matrix being non-invertible or the pseudo-inverse calculation being inaccurate. A low-rank matrix cannot provide sufficient spatial degrees of freedom to separate signals. When the number of channel paths reaches  $L=8$ , the secrecy rate tends to stabilize. At this critical point, the proposed scheme outperforms the Fixed IRS by 0.36 dB, the FPA by 0.16 dB, and the ZF by 0.67 dB, as clearly indicated by the visual annotations in the figure. This stabilization suggests that the channel paths' contribution to the secrecy rate reaches a saturation point, where further increases in path numbers yield diminishing gains in performance.

## V. CONCLUSION

This paper focused on an ISAC system for a single-target and single-user case, which was assisted by an intelligent reflecting surface and MA. The objective was to maximize the secure rate under the joint optimization of the communication beamformer at the transmitter, the sensing covariance matrix, the phase shifts of IRS, and the position of the MA. To solve this non-convex problem, a PSO based alternating algorithm was adopted. Finally, the simulation results demonstrated that the proposed scheme could achieve good effectiveness compared with other benchmarking schemes.

## REFERENCES

- [1] F. Liu, Y. Cui, C. Masouros, J. Xu, T. X. Han, Y. C. Eldar, and S. Buzzi, "Integrated sensing and communications: Toward dual-functional wireless networks for 6G and beyond," *IEEE J. Sel. Areas Commun.*, vol. 40, no. 6, pp. 1728-1767, Jun. 2022.

- [2] X. Yang, Z. Wei, J. Xu, Y. Fang, H. Wu, and Z. Feng, "Coordinated transmit beamforming for networked ISAC with imperfect CSI and time synchronization," *IEEE Trans. Wireless Commun.*, vol. 23, no. 12, pp. 18019-18035, Dec. 2024.
- [3] Q. Zhu, M. Li, R. Liu, and Q. Liu, "Cramér-Rao bound optimization for active IRS-empowered ISAC systems," *IEEE Trans. Wireless Commun.*, vol. 23, no. 9, pp. 11723-11736, Sep. 2024.
- [4] D. Zhang, Y. Cui, X. Cao, N. Su, F. Liu, X. Jing, J. A. Zhang, J. Xu, C. Masouros, D. Niyato, and M. D. Renzo, "Integrated sensing and communications over the years: An evolution perspective," *arXiv:2504.06830*, 2025.
- [5] Y. Cui, X. Cao, G. Zhu, J. Nie, and J. Xu, "Edge perception: Intelligent wireless sensing at network edge," *IEEE Commun. Mag.*, vol. 63, no. 3, pp. 166-173, Mar. 2025.
- [6] D. Wen, P. Liu, G. Zhu, Y. Shi, J. Xu, Y. C. Eldar, and S. Cui, "Task-oriented sensing, computation, and communication integration for multi-device edge AI," *IEEE Trans. Wireless Commun.*, vol. 23, no. 3, pp. 2486-2502, Mar. 2024.
- [7] X. Cao, Z. Lyu, G. Zhu, J. Xu, L. Xu, and S. Cui, "An overview on over-the-air federated edge learning," *IEEE Wireless Commun.*, vol. 31, no. 3, pp. 202-210, Jun. 2024.
- [8] Z. Liu, X. Chen, H. Wu, Z. Wang, X. Chen, D. Niyato, and K. Huang, "Integrated sensing and edge AI: Realizing intelligent perception in 6G," 2025. [Online]. Available: <https://arxiv.org/abs/2501.06726>
- [9] Z. Wang, K. Huang, and Y. C. Eldar, "Spectrum breathing: Protecting over-the-air federated learning against interference," *IEEE Trans. Wireless Commun.*, vol. 23, no. 8, pp. 10058-10071, 2024.
- [10] Z. Wang, Q. Zeng, H. Zheng, and K. Huang, "Revisiting outage for edge inference systems," 2025. [Online]. Available: <https://arxiv.org/abs/2504.03686>
- [11] B. K. Chalise, M. G. Amin, and B. Himed, "Performance tradeoff in a unified passive radar and communications system," *IEEE Signal Process. Lett.*, vol. 24, no. 9, pp. 1275-1279, Sep. 2017.
- [12] F. Liu, Y.-F. Liu, A. Li, C. Masouros, and Y. C. Eldar, "Cramér-Rao bound optimization for joint radar-communication beamforming," *IEEE Trans. Signal Process.*, vol. 70, pp. 240-253, 2022.
- [13] Y. Liu, H. Chen, and L. Wang, "Physical layer security for next generation wireless networks: Theories, technologies, and challenges," *IEEE Commun. Surveys Tutorials*, vol. 19, no. 1, pp. 347-376, Firstquarter 2017.
- [14] Y. Zou, J. Zhu, X. Wang, and L. Hanzo, "A survey on wireless security: Technical challenges, recent advances, and future trends," *Proc. IEEE*, vol. 104, no. 9, pp. 1727-1765, Sep. 2016.
- [15] J. Zou, C. Masouros, F. Liu, and S. Sun, "Securing the sensing functionality in ISAC networks: An artificial noise design," *IEEE Trans. Veh. Technol.*, vol. 73, no. 11, pp. 17800-17805, Nov. 2024.
- [16] K. Ren, H. Su, and Q. Wang, "Secret key generation exploiting channel characteristics in wireless communications," *IEEE Wireless Commun.*, vol. 18, no. 4, pp. 6-12, Aug. 2011.
- [17] K. Cao, B. Wang, H. Ding, L. Lv, R. Dong, and T. Cheng, "Improving physical layer security of uplink NOMA via energy harvesting jammers," *IEEE Trans. Inf. Forensics Security*, vol. 16, pp. 786-799, Sept. 2021.
- [18] B. He, F. Wang, and J. Cheng, "Joint secure transceiver design for integrated sensing and communication," *IEEE Trans. Wireless Commun.*, vol. 23, no. 10, pp. 13377-13393, Oct. 2024.
- [19] L. Zhu, W. Ma, and R. Zhang, "Modeling and performance analysis for movable antenna enabled wireless communications," *IEEE Trans. Wireless Commun.*, vol. 23, no. 6, pp. 6234-6250, Jun. 2024.
- [20] G. Hu, Q. Wu, D. Xu, K. Xu, J. Si, Y. Cai, and N. Al-Dhahir, "Movable antennas-assisted secure transmission without eavesdroppers' instantaneous CSI," *IEEE Trans. Mob. Comput.*, vol. 23, no. 12, pp. 14263-14279, Dec. 2024.
- [21] L. Zhu, W. Ma, B. Ning, and R. Zhang, "Movable-antenna enhanced multiuser communication via antenna position optimization," *IEEE Trans. Wireless Commun.*, vol. 23, no. 7, pp. 7214-7229, Jul. 2024.
- [22] J. Chen, K. Wu, J. Niu, Y. Li, P. Xu, and J. A. Zhang, "Spectral and energy efficient waveform design for IRS-assisted ISAC," *IEEE Trans. Commun.*, early access, 2024.
- [23] H. Zhou, Y. Liang, R. Long, L. Zhao, and Y. Pei, "Reconfigurable intelligent surface for FDD systems: Design and optimization," *IEEE Internet Things J.*, vol. 10, no. 11, pp. 9607-9621, Jun. 2023.
- [24] S. Kim, J. Wu, and B. Shim, "Efficient channel probing and phase shift control for mmWave reconfigurable intelligent surface-aided communications," *IEEE Trans. Wireless Commun.*, vol. 23, no. 1, pp. 231-246, Jan. 2024.
- [25] T. Wang, F. Fang, and Z. Ding, "An SCA and relaxation based energy efficiency optimization for multi-user IRS-assisted NOMA networks," *IEEE Trans. Veh. Technol.*, vol. 71, no. 6, pp. 6843-6847, Jun. 2022.
- [26] W. Zhang, K. Xiong, R. Zhang, P. Fan, and K. Ben Letaief, "SEE maximization in RIS-aided network with RSMA: A PPO-SCF method," *IEEE Wireless Commun. Lett.*, vol. 13, no. 12, pp. 3315-3319, Dec. 2024.
- [27] Y. Guo, J. Fan, R. Zhang, B. Chang, D. W. KwanNg, and D. Niyato, "Secrecy energy efficiency maximization in IRS-assisted VLC MISO networks with RSMA: A DS-PPO approach," *IEEE Trans. Wireless Commun.*, early access, 2025.
- [28] C. Zhong, J. Yao, and J. Xu, "Secure UAV communication with cooperative jamming and trajectory control," *IEEE Commun. Lett.*, vol. 23, no. 2, pp. 286-289, Feb. 2019.
- [29] J. Yao and J. Xu, "Joint 3D maneuver and power adaptation for secure UAV communication with CoMP reception," *IEEE Trans. Wireless Commun.*, vol. 19, no. 10, pp. 6992-7006, Oct. 2020.
- [30] W. Lu, Y. Mo, Y. Feng, Y. Gao, N. Zhao, Y. Wu, and A. Nallanathan, "Secure transmission for multi-UAV-assisted mobile edge computing based on reinforcement learning," *IEEE Trans. Network Sci. Eng.*, vol. 10, no. 3, pp. 1270-1282, Jun. 2023.
- [31] L. Guo, J. Jia, J. Chen, S. Yang, Y. Xue, and X. Wang, "RIS-aided secure A2G communications with coordinated multi-UAVs: A hybrid DRL approach," *IEEE Trans. Network Sci. Eng.*, vol. 11, no. 5, pp. 4536-4550, Sep. 2024.
- [32] B. Ji, Y. Wang, L. Xing, C. Li, Y. Wang, and H. Wen, "IRS-driven cybersecurity of healthcare cyber physical systems," *IEEE Trans. Network Sci. Eng.*, vol. 10, no. 5, pp. 2564-2573, Sep. 2023.
- [33] Y. Zhang, X. Gao, M. Shi, H. Yuan, J. Kang, D. Niyato, and K. Yang, "Robust secure UAV communications with the aid of jamming beamforming," *IEEE Trans. Commun.*, early access, 2025.
- [34] D. Zhou, L. Li, S. Gong, B. Gu, G. Chen, and D. Niyato, "Learning adaptive jamming and beamforming for hybrid IRS-assisted secure NOMA transmissions," *IEEE Trans. Commun.*, early access, 2025.
- [35] C. Jiang, C. Zhang, C. Huang, J. Ge, D. Niyato, and C. Yuen, "RIS-assisted ISAC systems for robust secure transmission with imperfect sense estimation," *IEEE Trans. Wireless Commun.*, early access, 2025.
- [36] J. Xu, X. Yu, L. Xu, C. Xing, N. Zhao, X. Wang, and D. Niyato, "IRS-UAV assisted secure integrated sensing and communication," *IEEE Wireless Commun.*, vol. 31, no. 5, pp. 61-67, Oct. 2024.
- [37] P. Liu, Z. Fei, X. Wang, B. Li, Y. Huang, and Z. Zhang, "Outage constrained robust secure beamforming in integrated sensing and communication systems," *IEEE Wireless Commun. Lett.*, vol. 11, no. 11, pp. 2260-2264, Nov. 2022.
- [38] J. Chu, R. Liu, M. Li, Y. Liu, and Q. Liu, "Joint secure transmit beamforming designs for integrated sensing and communication systems," *IEEE Trans. Veh. Technol.*, vol. 72, no. 4, pp. 4778-4791, Apr. 2023.
- [39] D. Xu, X. Yu, D. W. K. Ng, A. Schmeink, and R. Schober, "Robust and secure resource allocation for ISAC systems: A novel optimization framework for variable-length snapshots," *IEEE Trans. Commun.*, vol. 70, no. 12, pp. 8196-8214, Dec. 2022.
- [40] W. Wei, X. Pang, X. Qin, S. Gong, C. Xing, and N. Zhao, "Cramér-Rao bound and secure transmission trade-off design for semi-IRS-enabled ISAC," *IEEE Trans. Wireless Commun.*, vol. 23, no. 11, pp. 15753-15767, Nov. 2024.
- [41] J. Zhang, J. Xu, W. Lu, N. Zhao, X. Wang, and D. Niyato, "Secure transmission for IRS-aided UAV-ISAC networks," *IEEE Trans. Wireless Commun.*, vol. 23, no. 9, pp. 12256-12269, Sep. 2024.
- [42] X. Yu, J. Xu, N. Zhao, X. Wang, and D. Niyato, "Security enhancement of ISAC via IRS-UAV," *IEEE Trans. Wireless Commun.*, vol. 23, no. 10, pp. 15601-15612, Oct. 2024.
- [43] D. Li, Z. Yang, N. Zhao, Z. Wu and T. Q. S. Quek, "NOMA aided secure transmission for IRS-ISAC," *IEEE Trans. Wireless Commun.*, vol. 23, no. 9, pp. 10911-10925, Sep. 2024.
- [44] M. Hua, Q. Wu, W. Chen, O. A. Dobre, and A. L. Swindlehurst, "Secure intelligent reflecting surface-aided integrated sensing and communication," *IEEE Trans. Wireless Commun.*, vol. 23, no. 1, pp. 575-591, Jan. 2024.
- [45] X. Yu, J. Xu, X. Qin, J. Tang, N. Zhao, and D. Niyato, "Multistatic cooperative sensing assisted secure transmission via IRS," *IEEE Trans. Wireless Commun.*, early access, 2025.
- [46] W. Wei, X. Pang, C. Xing, N. Zhao, and D. Niyato, "STAR-IRS aided secure NOMA integrated sensing and communication," *IEEE Trans. Wireless Commun.*, vol. 23, no. 9, pp. 10712-10725, Sep. 2024.
- [47] T. Zhou, K. Xu, G. Hu, X. Xia, C. Li, C. Wei, and C. Liao, "Robust and secure beamforming design for STAR-RIS-enabled IoT ISAC systems," *IEEE Internet Things J.*, vol. 12, no. 7, pp. 8742-8758, Apr. 2025.



- [48] Z. Yang, S. Zhang, G. Chen, Z. Dong, Y. Wu, and D. B. d. Costa, "Secure integrated sensing and communication systems assisted by active RIS," *IEEE Trans. Veh. Technol.*, vol. 73, no. 12, pp. 19791-19796, Dec. 2024.
- [49] Z. Yang, S. Zhang, G. Chen, Z. Dong, Y. Wu, and D. Benevides da Costa, "Secure wireless communication in active RIS-assisted DFRC Systems," *IEEE Trans. Veh. Technol.*, vol. 74, no. 1, pp. 626-640, Jan. 2025.
- [50] Q. Liu, Y. Zhu, M. Li, R. Liu, Y. Liu, and Z. Lu, "DRL-based secrecy rate optimization for IRS-assisted secure ISAC systems," *IEEE Trans. Veh. Technol.*, vol. 72, no. 12, pp. 16871-16875, Dec. 2023.
- [51] L. Zhu, W. Ma, and R. Zhang, "Movable-antenna array enhanced beamforming: Achieving full array gain with null steering," *IEEE Commun. Lett.*, vol. 27, no. 12, pp. 3340-3344, Dec. 2023.
- [52] W. Xiong, K. Zhong, Z. Xiao, J. Lin, and Q. Li, "Secure analog beamforming design for wireless communication systems with movable antennas," in *Proc. of ICASSP 2025*, Hyderabad, India, 2025, pp. 1-5.
- [53] N. Li, P. Wu, B. Ning, and L. Zhu, "Sum rate maximization for movable antenna enabled uplink NOMA," *IEEE Wireless Commun. Lett.*, vol. 13, no. 8, pp. 2140-2144, Aug. 2024.
- [54] Y. Wu, D. Xu, D. W. K. Ng, W. Gerstacker, and R. Schober, "Movable antenna-enhanced multiuser communication: Jointly optimal discrete antenna positioning and beamforming," in *Proc. GLOBECOM 2023-2023 IEEE Global Communications Conference*, Kuala Lumpur, Malaysia, 2023, pp. 7508-7513.
- [55] G. Hu, Q. Wu, D. Xu, K. Xu, J. Si, Y. Cai, and N. Al-Dhahir, "Intelligent reflecting surface-aided wireless communication with movable elements," *IEEE Wireless Commun. Lett.*, vol. 13, no. 4, pp. 1173-1177, Apr. 2024.
- [56] J. Xiao, Y. Liu, Y. Chen, X. Wu, and F. Hou, "Throughput maximization for movable antenna and IRS enhanced wireless powered IoT networks," in *Proc. 2024 IEEE Wireless Communications and Networking Conference (WCNC)*, Dubai, United Arab Emirates, 2024, pp. 1-6.
- [57] H. Wu, H. Ren, C. Pan, and Y. Zhang, "Movable antenna-enabled RIS-aided integrated sensing and communication," *arXiv:2407.03228*, Sep. 2024.
- [58] H. Qin, W. Chen, Q. Wu, Z. Zhang, Z. Li, and N. Cheng, "Cramér-Rao bound minimization for movable antenna-assisted multiuser integrated sensing and communications," *IEEE Wireless Commun. Lett.*, vol. 13, no. 12, pp. 3404-3408, Dec. 2024.
- [59] C. Jiang, C. Zhang, C. Huang, J. Ge, D. Niyato, and C. Yuen, "Movable antenna-assisted integrated sensing and communication systems," *IEEE Trans. Wireless Commun.*, early access, 2025.
- [60] H. Wu, H. Ren, C. Pan, and Y. Zhang, "Movable antenna-enabled RIS-aided integrated sensing and communication," *IEEE Trans. Cognit. Commun. Networking*, early access, 2025.
- [61] W. Xiang, Y. Chen, X. Zhang, Z. Lu, and X. Wen, "Joint antenna position and transmit signal optimization for ISAC system with movable antenna array," in *Proc. 2024 IEEE 35th International Symposium on Personal, Indoor and Mobile Radio Communications (PIMRC)*, Valencia, Spain, 2024, pp. 1-6.
- [62] W. Lyu, S. Yang, Y. Xiu, Z. Zhang, C. Assi, and C. Yuen, "Flexible beamforming for movable antenna-enabled integrated sensing and communication," *arXiv:2405.10507*, 2024.
- [63] W. Lyu, S. Yang, Y. Xiu, Z. Zhang, C. Assi, and C. Yuen, "Movable antenna enabled integrated sensing and communication," *IEEE Trans. Wirel. Commun.*, early access, 2025.
- [64] S. Zhang and R. Zhang, "Capacity characterization for intelligent reflecting surface aided MIMO communication," *IEEE J. Sel. Areas Commun.*, vol. 38, no. 8, pp. 1823-1838, Aug. 2020.
- [65] Q. Wu and R. Zhang, "Beamforming optimization for wireless network aided by intelligent reflecting surface with discrete phase shifts," *IEEE Trans. Commun.*, vol. 68, no. 3, pp. 1838-1851, Mar. 2020.
- [66] Y. Fang, S. Zhang, X. Li, X. Yu, J. Xu, and S. Cui, "Multi-IRS-enabled integrated sensing and communications," *IEEE Trans. Wireless Commun.*, vol. 72, no. 9, pp. 5853-5867, Sep. 2024.
- [67] J. Zuo, Y. Liu, C. Zhu, Y. Zou, D. Zhang, and N. Al-Dhahir, "Exploiting NOMA and IRS in integrated sensing and communication," *IEEE Trans. Veh. Technol.*, vol. 72, pp. 12941-12955, May 2023.
- [68] Z. Xiao, X. Pi, L. Zhu, X. G. Xia, and R. Zhang, "Multiuser communications with movable-antenna base station: Joint antenna positioning, receive combining, and power control," *IEEE Trans. Wireless Commun.*, early access, 2024.



**Xiaowen Cao** received the B.Eng. and Ph.D. degrees from the Guangdong University of Technology in 2017 and 2022, respectively. She is now an assistant professor in College of Electronics and Information Engineering, Shenzhen University, Shenzhen, China, and a visiting scholar in Guangdong Provincial Key Laboratory of Future Networks of Intelligence, Shenzhen, China. Her research interests include edge learning, over-the-air computation, as well as integrated sensing, communication, and computation. She is a recipient of the World's Top 2% Scientists by Stanford University, the Best Paper Award of IEEE JC&S 2024, and the eExemplary Reviewer for IEEE WCL. She has served as a Co-Chair of IEEE VTC-fall 2023 workshop on ISCC, and a TPC Co-Chair of IEEE WCNC/PIMRC 2024 workshop.



**Peng Jiang** received the M.S. degree in electronic information with the College of Electronics and Information Engineering, Shenzhen University, Shenzhen, China. His research interests include wireless communications and intelligent reflecting surface.



**Guangxu Zhu** received the Ph.D. degree in electrical and electronic engineering from The University of Hong Kong in 2019. Currently he is a senior research scientist and deputy director of network system optimization center at the Shenzhen research institute of big data, and an adjunct associate professor with the Chinese University of Hong Kong, Shenzhen. His recent research interests include edge intelligence, semantic communications, and integrated sensing and communication. He is a recipient of the 2023 IEEE ComSoc Asia-Pacific Best Young Researcher Award and Outstanding Paper Award, the World's Top 2% Scientists by Stanford University, the "AI 2000 Most Influential Scholar Award Honorable Mention", the Young Scientist Award from UCOM 2023, the Best Paper Award from WCSP 2013 and IEEE JS&C 2024. He serves as associate editors at top-tier journals in IEEE, including IEEE TMC, TWC and WCL. He is the vice co-chair of the IEEE ComSoc Asia-Pacific Board Young Professionals Committee.



**Yejun He** (Senior Member, IEEE) received the Ph.D. degree in Information and Communication Engineering from the Huazhong University of Science and Technology (HUST), Wuhan, China, in 2005. From 2005 to 2006, he was a Research Associate with the Department of Electronic and Information Engineering, The Hong Kong Polytechnic University, Hong Kong. From 2006 to 2007, he was a Research Associate with the Department of Electronic Engineering, Faculty of Engineering, The Chinese University of Hong Kong, Hong Kong. In 2012, he joined the Department of Electrical and Computer Engineering, University of Waterloo, Waterloo, ON, Canada, as a Visiting Professor. From 2013 to 2015, he was an Advanced Visiting Scholar (Visiting Professor) with the School of Electrical and Computer Engineering, Georgia Institute of Technology, Atlanta, GA, USA. From 2023 to 2024, he was an Advanced Research Scholar (Visiting Professor) with the Department of Electrical and Computer Engineering, National University of Singapore, Singapore.

Since 2006, he has been a faculty of Shenzhen University, where he is currently a Full Professor with the College of Electronics and Information Engineering, Shenzhen University, Shenzhen, China, the Director of Sino-British Antennas and Propagation Joint Laboratory of Ministry of Science and Technology of the People's Republic of China (MOST), the Director of the Guangdong Engineering Research Center of Base Station Antennas and Propagation, and the Director of the Shenzhen Key Laboratory of Antennas and Propagation. He was selected as an Expert with Special Government Allowance from the State Council in China, and a Leading Talent in the "Guangdong Special Support Program" in 2024. He was promoted to the Shenzhen "Pengcheng Scholar" Distinguished Professor in 2020. He has authored or coauthored more than 350 refereed journal and conference papers and seven books. He holds more than 30 patents. His research interests include wireless communications, antennas, and radio frequency.

Dr. He was also a recipient of the Shenzhen Overseas High-Caliber Personnel Level B (Peacock Plan Award B) and Shenzhen High-Level Professional Talent (Local Leading Talent). He received the Second Prize of Shenzhen Science and Technology Progress Award in 2017, the Three Prize of Guangdong Provincial Science and Technology Progress Award in 2018, the Second Prize of Guangdong Provincial Science and Technology Progress Award in 2023, and the 10th Guangdong Provincial Patent Excellence Award in 2023. He is currently the Chair of IEEE Antennas and Propagation Society-Shenzhen Chapter and obtained the 2022 IEEE APS Outstanding Chapter Award. He has served as a Technical Program Committee Member or a Session Chair for various conferences, including the IEEE Global Telecommunications Conference (GLOBECOM), the IEEE International Conference on Communications (ICC), the IEEE Wireless Communication Networking Conference (WCNC), and the IEEE Vehicular Technology Conference (VTC). He served as the TPC Chair for IEEE ComComAp 2021 and the General Chair for IEEE ComComAp 2019. He was selected as a Board Member of the IEEE Wireless and Optical Communications Conference (WOCC). He served as the TPC Co-Chair for WOCC 2023/2022/2019/2015, APCAP 2023, UCMMT 2023, ACES-China2023, NEMO 2020 and so on. He acted as the Publicity Chair of several international conferences such as the IEEE PIMRC 2012. He has served as an Executive Chair of 2024/2025 IEEE International Workshop of Radio Frequency and Antenna Technologies. He is the Principal Investigator for over 40 current or finished research projects, including the National Natural Science Foundation of China, the Science and Technology Program of Guangdong Province, and the Science and Technology Program of Shenzhen City. He has served as a Reviewer for various journals, such as the IEEE Transactions on Vehicular Technology, the IEEE Transactions on Communications, the IEEE Transactions on Industrial Electronics, the IEEE Transactions on Antennas and Propagation, the IEEE Wireless Communications, the IEEE Communications Letters, the International Journal of Communication Systems, and Wireless Personal Communications.

Dr. He is a Fellow of IET, and a Fellow of China Institute of Communications (CIC). He is serving as an Associate Editor for IEEE Transactions on Vehicular Technology, IEEE Transactions on Antennas and Propagation, IEEE Transactions on Mobile Computing, IEEE Antennas and Wireless Propagation Letters, IEEE Antennas and Propagation Magazine, International Journal of Communication Systems, China Communications, and ZTE Communications.



**Mohsen Guizani** (Fellow, IEEE) received the BS (with distinction), MS and PhD degrees in Electrical and Computer engineering from Syracuse University, Syracuse, NY, USA in 1985, 1987 and 1990, respectively. He is currently a Professor of Machine Learning and the Associate Provost at Mohamed Bin Zayed University of Artificial Intelligence (MBZUAI), Abu Dhabi, UAE. Previously, he worked in different institutions in the USA. His research interests include applied machine learning and artificial intelligence, Internet of Things (IoT),

intelligent autonomous systems, smart city, and cybersecurity. He was elevated to the IEEE Fellow in 2009 and was listed as a Clarivate Analytics Highly Cited Researcher in Computer Science in 2019, 2020 and 2021. Dr. Guizani has won several research awards including the "2015 IEEE Communications Society Best Survey Paper Award", the Best ComSoc Journal Paper Award in 2021 as well five Best Paper Awards from ICC and Globecom Conferences. He is the author of ten books and more than 800 publications. He is also the recipient of the 2017 IEEE Communications Society Wireless Technical Committee (WTC) Recognition Award, the 2018 AdHoc Technical Committee Recognition Award, and the 2019 IEEE Communications and Information Security Technical Recognition (CISTC) Award. He served as the Editor-in-Chief of IEEE Network and is currently serving on the Editorial Boards of many IEEE Transactions and Magazines. He was the Chair of the IEEE Communications Society Wireless Technical Committee and the Chair of the TAOS Technical Committee. He served as the IEEE Computer Society Distinguished Speaker and is currently the IEEE ComSoc Distinguished Lecturer. Mohsen Guizani (M'89-SM'99-F'09) received the BS (with distinction), MS and PhD degrees in Electrical and Computer engineering from Syracuse University, Syracuse, NY, USA in 1985, 1987 and 1990, respectively. He is currently a Professor of Machine Learning and the Associate Provost at Mohamed Bin Zayed University of Artificial Intelligence (MBZUAI), Abu Dhabi, UAE. Previously, he worked in different institutions in the USA. His research interests include applied machine learning and artificial intelligence, Internet of Things (IoT), intelligent autonomous systems, smart city, and cybersecurity. He was elevated to the IEEE Fellow in 2009 and was listed as a Clarivate Analytics Highly Cited Researcher in Computer Science in 2019, 2020 and 2021. Dr. Guizani has won several research awards including the "2015 IEEE Communications Society Best Survey Paper Award", the Best ComSoc Journal Paper Award in 2021 as well five Best Paper Awards from ICC and Globecom Conferences. He is the author of ten books and more than 800 publications. He is also the recipient of the 2017 IEEE Communications Society Wireless Technical Committee (WTC) Recognition Award, the 2018 AdHoc Technical Committee Recognition Award, and the 2019 IEEE Communications and Information Security Technical Recognition (CISTC) Award. He served as the Editor-in-Chief of IEEE Network and is currently serving on the Editorial Boards of many IEEE Transactions and Magazines. He was the Chair of the IEEE Communications Society Wireless Technical Committee and the Chair of the TAOS Technical Committee. He served as the IEEE Computer Society Distinguished Speaker and is currently the IEEE ComSoc Distinguished Lecturer.